Origin of Triassic magmatism of the Southern Alps (Italy): Constraints from geochemistry and Sr-Nd-Pb isotopic ratios

Michele Lustrino, Hassan Abbas, Samuele Agostini, Marcello Caggiati, Eugenio Carminati, Piero Gianolla

PII: S1342-937X(19)30142-X
DOI: https://doi.org/10.1016/j.gr.2019.04.011
Reference: GR 2149

To appear in: *Gondwana Research*

Received date: 28 September 2018
Revised date: 14 April 2019
Accepted date: 16 April 2019

Please cite this article as: M. Lustrino, H. Abbas, S. Agostini, et al., Origin of Triassic magmatism of the Southern Alps (Italy): Constraints from geochemistry and Sr-Nd-Pb isotopic ratios, Gondwana Research, https://doi.org/10.1016/j.gr.2019.04.011

Origin of Triassic magmatism of the Southern Alps (Italy): constraints from geochemistry and Sr-Nd-Pb isotopic ratios

Michele Lustrino[1,2]*, Hassan Abbas[1], Samuele Agostini[3], Marcello Caggiati[4], Eugenio Carminati[1], Piero Gianolla[4]

1 = Dipartimento di Scienze della Terra, Sapienza Università di Roma, P.le A. Moro 5, 00185, Roma, Italy
2 = Istituto di Geologia Ambientale e Geoingegneria (CNR – IGAG) c/o Dipartimento di Scienze della Terra, Sapienza Università di Roma, P.le A. Moro, 5, 00185 Roma, Italy
3 = Istituto di Geoscienze e Georisorse (CNR – IGG), Via Moruzzi 1, 56124, Pisa, Italy
4 = Dipartimento di Fisica e Scienze della Terra, Università degli studi di Ferrara, Via Saragat 1, 44122, Ferrara, Italy

* = Corresponding author. E-mail: michele.lustrino@uniroma1.it

Key-words: Dolomites, Ladinian magmatism, Petrogenesis, Geochemistry, Geodynamics

Abstract

During Middle-early Late Triassic (~243-235 Ma) a diffuse igneous activity developed in the Southern Alps (Italy). Sparse lava flow and pyroclastic succession remnants of such Southern Alps Triassic Igneous Rocks (SATIR) crop out in the Brescian pre-Alps, the Vicentinian Alps (Recoaro-Schio-Posina), Non Valley, Dolomites and Julian Alps. Plutonic rocks are found in two main plutonic complexes (Monzoni and Predazzo) and a small stock (Cima di Pape). Coeval igneous products can be traced eastward to Austria and Dinarides, for a total length of ~450 km.

The coeval formation of major late Anisian-late Ladinian carbonate platforms in the subsiding eastern Dolomites, and significant uplift and subaerial erosion in the western Dolomites suggest, for these areas, the occurrence of large-scale strike-slip and extensional tectonics with the development of horst-and-graben structures.

This study reports the first complete review of the SATIR activity, including new mineral chemical data on 14 samples, 61 major and trace element whole rock analyses and 7 Sr-Nd-Pb isotopic ratios for volcanic and plutonic samples from Dolomites (lavas plus Monzoni and Predazzo plutonic rocks) and Vicentinian Alps lavas. Despite the variable post-magmatic modifications, the large areal distribution of the products and their wide spectrum of chemical compositions, these samples show rather common geochemical and mineralogical characteristics and define major and trace element trends that can be associated with nearly close-system

magmatic evolution. Minor upper crustal contaminations can be observed in specific cases, mostly in the most differentiated products (SiO_2 >70 wt%).

A specific characteristic of SATIR is their calcalkaline to shoshonitic affinity, resembling the derivation from subduction-modified mantle sources, a feature at odds with the coeval strike-slip and extensional tectonics. Geochemical modelling, petrological considerations and geological constraints allow us to propose a model in which the SATIR mantle sources reflect previous subduction metasomatism (likely occurred during Variscan times). These metasomatised mantle sources were reactivated ~90-100 Myr after the end of the subduction, when continental rifting caused a raise of the geotherms and passive upwelling of asthenospheric mantle.

Keywords: Dolomites, Triassic, Gondwana, Continental rifting, Petrology

1. Introduction

Magmas generated in active subduction settings usually show peculiar volcanological, petrographic, mineral chemical, geochemical and isotopic characteristics, commonly very different from those emplaced in intra-plate settings and along passive plate margins (e.g., Lustrino et al., 2011; Turner and Langmuir, 2015; Di Giuseppe et al., 2017; Kimura, 2017; Schmidt and Jagoutz, 2017; Zheng and Zhao, 2017). However, the use geochemical data and petrological arguments to infer a given tectonic setting does not always guarantee correct conclusions. Indeed, compositions found along active plate margins, falling in the calcalkaline, high-K calcalkaline and potassic-ultrapotassic series are also recorded in intra-plate settings and in extensional areas post-dating subduction processes (Davidson, 1996; Turner et al., 1996; Liegeois et al., 1998; Fan et al., 2003; Moghazi, 2003; Lan et al., 2012; Lustrino et al., 2016).

If geological and geophysical data (e.g., earthquake distribution, focal mechanisms, mantle tomography) can help unravelling the geodynamic setting of active to recent magmatism, similar constraints are hard to obtain for the geological past. Thus, when dealing with remnants of past igneous activity, Earth scientists work mostly with geochemical data, using petrographic evidences and inferring petrological reasoning, helped by geological and structural constraints. The multidisciplinary approach could drive to non-unique definitions of the geodynamic processes responsible for magmatism in the past, because geological s.l. (i.e., stratigraphy, structural geology) and geochemical-petrological interpretations do not always match.

A case study is represented by the Middle-Late Triassic igneous activity occurred coeval to strike-slip and extensional tectonics in the Southern Alps (northern Italy; e.g., Doglioni, 1992; Bertotti et al. 1993; Gianolla et al., 1998; Brandner et al., 2016; Abbas et al., 2018) and adjoining regions (Carinthia, Po Plain, Adriatic Sea and Dinarides), for a total width of ~450 km (Fig. 1). The Italian products of this phase

investigated in this study are hereafter abbreviated into SATIR (Southern Alps Triassic Igneous Rocks). SATIR show calcalkaline to shoshonitic affinities, at odds with geological evidence, which indicates coeval strike-slip and extensional tectonics. This renders the geodynamic framework in which SATIR originated still a matter of discussion (e.g., Sloman, 1989).

A long list of geodynamic and tectonic scenarios to explain the middle Triassic tectonic and magmatic activity in the Dolomites and whole Southern Alps was proposed in the literature. These can be grouped as follows (Abbas et al., 2018): *1)* aborted continental rifting – based on the association of extensional structures and mafic volcanism (Bechstadt et al., 1977); *2)* Northward subduction of lower continental crust in the upper mantle (Castellarin et al., 1988) – based on the calcalkaline and shoshonitic magmatic association; *3)* Sinistral strike-slip tectonics – based on the association of compressional and extensional structures with volcanic and plutonic intrusions (Blendinger, 1985; Doglioni, 1987, 1988); *4)* Heritage of ancient subduction events of Variscan age, coupled with assimilation of upper crustal rocks (Crisci et al., 1984; Sloman, 1989; Bonadiman et al., 1994; Beccaluva et al., 2005); *5)* Development of a marginal back-arc basin associated with the post-Variscan evolution of the Alpine sector (Marinelli et al. 1980; Viel, 1982); *6)* Intra-Pangea dextral mega-shear system with lithosphere-scale extension enabling hybridization between mantle melts and lower crust lithologies (Brandner and Keim, 2011); *7)* Active upwelling of hot asthenospheric mantle (Stahle et al., 2001); *8)* Subduction of small Permian back-arc oceanic basins (Garzanti 1985; Zanetti et al. 2013); *9)* Extension-related magmatism during the Middle Triassic in the Southern and Eastern Alps following the opening of Meliata Ocean (Brandner et al., 2016; Beltrán-Trivinõ et al., 2016); *10)* Active arc/back-arc development following the NNW-directed subduction of the Paleotethys oceanic lithosphere beneath the south-eastern European paleo-margin (Cassinis et al., 2008); *11)* closure, by a subduction dipping beneath the Southalpine, of a Paleozoic rifted continental basin or a narrow oceanic basin, located between the Southalpine and Austroalpine continental blocks, (Bianchini et al., 2018).

In this work we provide new petrographic, mineral chemical, whole-rock chemical and Sr-Nd-Pb isotope data of Ladinian lava flows, dykes and plutonic rocks from the Dolomites and Vicentinian Alps (Recoaro-Schio-Posina area). The aim is their characterisation from a petrological point of view for a better comprehension of the geodynamic framework in which they were emplaced. These data are discussed in the framework of a general review of the entire Triassic igneous activity of the Southern Alps and adjoining regions, based on a comprehensive dataset containing more than 1000 whole-rock data (provided as electronic appendix). Such a regional approach allows us to better constrain the mantle sources and discuss the geodynamic origin of Middle-Late Triassic igneous activity.

2. Geological setting

The Southern Alps (Fig. 1) are located south of the Neogene Periadriatic Line, a S-shaped NE-SW-trending dextral mylonitic shear zone separating Europe-verging thrusts to the north from Adria-verging thrusts to the south (Handy et al., 2010). The Southern Alps (i.e., the part of the Alps located south of the Periadriatic line) are considered in the literature as the retro-wedge of the double-verging Alpine Chain. They consist of a well-preserved Mesozoic passive continental margin (e.g., Bertotti et al., 1993), inverted during the Alpine Orogenesis (Doglioni, 1987; Handy et al., 2010). Their structuration initiated during the Cretaceous-Paleogene subduction of an eastern branch of the Alpine Tethys. This belt widened as a consequence of the Eocene Europe-Adria collision (Handy et al., 2010; Carminati et al., 2012; Carminati and Doglioni, 2012).

The Dolomites (Figs. 1 and 2) consist of a large-scale Neogene pop-up structure bounded by two main tectonic lineaments belonging to the Periadriatic Line: the dextrally transpressive Pusteria Line to the north, and the SSE-verging thrust of the Valsugana Line to the south. The Recoaro area lies in a more external wedge of the Southern Alps (Figs. 1 and 2), separated from the Cenozoic Veneto magmatic province to the south by the Cima Marana thrust, and affected to the east by the post-Miocene Schio-Vicenza and Val d'Astico sinistral strike-slip fault system (Castellarin et al., 2006, Fondriest et al., 2012).

3. Permian to Middle Triassic stratigraphy of the Dolomites

During Carboniferous time, the agglutination of Gondwana and Laurussia led to the formation of the Appalachian-Variscan Belt (e.g., Bell and Newman, 2006; Franke et al., 2017). The subduction of the Rheic Ocean, once separating northern Gondwana from southern Laurussia, led to the development of abundant Permian magmatism peaking during Early Permian (~300 ± 20 Ma).

The Dolomites sedimentary succession unconformably overlies these Permian volcanic rocks or directly older basement rocks (Massari and Neri, 1997; Brandner and Keim, 2011). Late Permian red-beds (Val Gardena Fm.) and evaporites/carbonates (Bellerophon Fm.; Bosellini and Hardie, 1973; Massari and Neri, 1997; Kustatscher et al., 2017) were followed by Early Triassic shallow-water carbonate and siliciclastic deposits (Werfen Fm. and Lower Serla Dolomite).

Late Anisian tectonics disrupted the Contrin carbonate platform and was followed by a strong regional subsidence. Isolated carbonate platforms nucleated and survived from the Late Anisian to Late Ladinian, facing deep water basins (Sciliar and Buchenstein Fm.; Maurer and Schlager, 2000; Preto et al., 2005; Brack et al., 2007; Stefani et al., 2010). Starting from the early Ladinian, but with a climax in late Ladinian, widespread magmatism occurred in the Southern Alps, now preserved as lava flows, pyroclastitic (including epiclastitic) and plutonic rocks. Local magma intrusions (Predazzo, Monzoni and Cima Pape; Lucchini et al., 1982; Bonadiman et

al., 1994; Visonà, 1997; Casetta et al., 2018a, 2018b; Abbas et al., 2018) occurring in the Dolomites were possibly related to subaerial volcanoes (Calanchi et al., 1978; Castellarin et al., 1982).

Ladinian volcanic rocks accumulated mostly in basinal depressions and onlapped the carbonate platform slopes (e.g., Sacerdoti and Sommavilla, 1962; Neri et al., 2007), while magmatic dykes intruded carbonate platform deposits (Vardabasso, 1930; Bosellini et al., 1982; Doglioni, 1983; Brandner and Keim, 2011). While close to the magmatic centers (e.g., Latemar and Marmolada areas) the carbonate platforms were buried beneath the volcanic products and demised, in other areas, still not far from magmatic centers (e.g., Sciliar Massif), carbonate production continued (De Zanche et al., 1993; Brandner and Keim, 2011). The erosion of volcanics led to deposition of coarse (e.g., Marmolada Conglomerate) to fine (Wengen Fm.) clastic deposits (Gianolla and Neri, 2007).

As widely discussed in the following sections, roughly coeval magmatism is recorded also in the Julian Alps (e.g., Spadea, 1970; Lucchini et al., 1980; Gianolla et al., 1992), Vicentinian Alps (e.g., Barbieri et al., 1982; De Vecchi and Sedea, 1983) and Brescian Prealps (e.g., Cassinis and Zezza, 1982; Armienti et al., 2003; Cassinis et al., 2008, 2011). At the end of the magmatic pulse, carbonate deposition fully re-established and several carbonate platforms (Cassian Dolomite) developed, prograding onto coeval basinal deposits (San Cassiano Fm.; Gianolla et al., 1998; Neri et al., 2007; Keim et al., 2001).

4. Pre-Cenozoic magmatism in the Southern Alps and adjoining areas

4.1. Permian magmatism

In the central-eastern Southern Alps, the Permian medium to high-K calcalkaline magmatism consists of volcanic rock piles (Athesian volcanism) and plutons (Cima d'Asta, Bressanone, Ivigna, Monte Croce and Monte Sabion; e.g., Macera et al., 1994; Rottura et al., 1997, 1998; Marocchi et al., 2008; Schaltegger and Brack, 2007; Bellieni et al., 2010). In the western and central Southern Alps, the Permian magmatism is represented by Ivrea Mafic Complex, the "Graniti dei Laghi" and the Lugano volcanics (e.g., Boriani et al., 1992; Pinarelli et al., 2002; Quick et al., 2009). This activity is mostly represented by bimodal calcalkaline to high-K calcalkaline products (e.g., Cocherie et al., 1994; Cortesogno et al., 1998; Romer et al., 2001; Perini et al., 2004; Kroner and Romer, 2013; Casini et al., 2015; Willcock et al., 2015; Gaggero et al., 2017; Braid et al., 2018), albeit sodic alkaline basic compositions are also present, principally in the last stages (e.g., Neumann et al., 2004).

4.2. Triassic magmatism

Scattered Middle Triassic magmatic rocks crop out in several areas along the Alps and the Dinarides. The following discussion will be restricted to the Southern Alps,

where Middle Triassic igneous rocks are widely recorded (Fig. 1). Magmatic activity started with Anisian acid volcanic rocks restricted to small outcrops in eastern Carnia (Rio Turriea and Gartnerkofel; e.g., Obenholzner and Pfeiffer, 1991; Venturini, 2006) and in southern Karawanken (Loibl pass; Buser, 1980). Upper Anisian to lower Ladinian porphyritic and plutonic rocks are more common in the eastern Southern Alps. The volume of these volcanic products increases eastward from the western Julian Alps (Rio Freddo, Prisjonik; Lucchini et al., 1980; Gianolla, 1992; Celarc et al., 2013) to the southern Karawanken, Tolmin Basin and to the Kamnik-Savinja Alps (Buser, 1980, 1986; Pamic, 1984; Visonà and Zanferrari, 2000; Dozet and Buser, 2009). Acid pyroclastic rocks are however frequent in the whole Southern Alps and occur as "Pietra Verde" tuff layers or ash interbeds in basinal limestones of Buchenstein Fm. (Viel, 1979; Cros, 1980; Brack and Rieber, 1993; Maurer, 2003; Wotzlaw et al., 2017).

Upper Ladinian volcanic rocks are very common (both in basinal and shelf settings) in the western and central Dolomites (Figs. 1, 2; Pisa et al., 1980; Bosellini et al., 1982; Sloman, 1989), along the western side of the Adige Valley (Mendola massif and Non Valley; Rossi et al., 1980; Avanzini et al., 2007), and in the Vicentinian Prealps (Recoaro-Schio-Posina; Barbieri et al., 1982; De Vecchi et al., 1986). Small outcrops occur also in western Carnia (Forni di Sopra; Castellarin and Pisa, 1973) and in the Brescian Prealps (Monte Guglielmo group; Cassinis et al., 2008, 2011). In addition, Middle Triassic (mainly Ladinian) magmatism has been recognised in boreholes drilled in the Po Plain and in the Adriatic Sea (Fig. 1; Brusca et al., 1982; Castellarin et al., 1988).

In the Dolomites, the age of late Ladinian volcanic rocks can be constrained by a well-defined bio-chronostratigraphic framework (Gianolla et al., 1998; Brack and Muttoni, 2000; Wotzlaw et al., 2017; Abbas et al., 2018; Maron et al., 2019; Storck et al., 2019) and by geochronological U-Pb-dating. Zircons from volcanic ash beds interbedded in the underlying Buchenstein Fm., in syn-volcanic clastics (Fernazza Fm.) and in the mainly post-volcanic Wengen Fm. (Mundil et al., 1996; Brack et al., 1997, 2007; Mietto et al., 2012; Wotzlaw et al., 2017; Storck et al., 2019) allows us to bracket the time interval of basaltic volcanism in the Dolomites between 239.044 ± 0.038 Ma (Wotzlaw et al., 2017) and 237.773 ± 0.052 Ma (Seiser Alm in Mietto et al., 2012). According to Storck et al. (2019) the duration of the paroxysmal phase of Ladinian volcanism in the Dolomites lasted less than 0.87 ± 0.06 Myr, in agreement with a short-lived Late Ladinian magmatic Event (Brandner et al., 2016; Abbas et al., 2018).

The ages of intrusive rocks have been recently updated by Storck et al. (2019) through high-quality Zircon U-Pb datings of the monzonitic intrusions and the syenitic dykes from Predazzo and Monzoni (ages between 238.190 ± 0.050 and 238.075 ± 0.087 Ma). These ages, together with the data of the Predazzo granite

(237.3 ± 1.0 Ma from mechanically abraded zircon; Brack et al., 1997 and 2005) indicate an equivalent age for intrusive and effusive products.

Lower Carnian magmatism is recorded also in the western Southern Alps (Brescian Prealps), with both effusive and intrusive products (Cassinis et al., 2008). A possible occurrence of coeval volcanic edifices more to the south is suggested by the occurrence of very common Lower Carnian volcaniclastic sandstones (Val Sabbia Ss., Garzanti, 1985; Jadoul et al., 2004; Cassinis et al., 2011).

5. Tectonic evolution of the Dolomites

The main tectonic events recorded in the Dolomites area can be resumed as follows: *1)* Permian-Triassic strike-slip and extensional tectonics (details below); *2)* nearly amagmatic Jurassic rifting associated with the opening of the Alpine Tethys Ocean; *3)* Paleogene ENE-WSW thin-skinned shortening related to the Europe-Adria plates convergence, which generated WSW-verging thrusts, N-S or NNW-SSE trending folds and conjugate strike-slip faults (Doglioni, 1987); *4)* Late Oligocene to Recent NNW-SSE thick-skinned shortening, which produced SSE-verging thrusting (Caputo et al., 2010).

Evidence for Middle Triassic tectonics in the Dolomites is provided by sinistral strike-slip faults oriented N70-90 (Stava, Trodena and Cavalase Lines; Abbas et al., 2018) associated with positive flower structures (Cima Bocche Anticline; Doglioni, 1983) and diapirs involving Late Permian evaporites (Bellerophon Fm.; Bechstadt et al., 1977; Pisa et al., 1980; Bosellini et al., 1982; Doglioni 1984, 1987; Castellarin et al., 1998; Doglioni and Carminati, 2008). These structures displace both basement and sedimentary successions up to the lower-middle Ladinian (Doglioni 1984, 1987; Doglioni and Carminati, 2008). Middle Triassic tectonics and coeval subsidence were ascribed to sinistral movements between Adria and Europe (Doglioni 1984, 1987).

Well-dated volcanic dykes, lava flows and plutonic bodies crosscut Triassic structures (thrusts, folds and diapirs) confirming their middle Triassic (late Ladinian) age (Doglioni 1984, 1987; Castellarin et al., 1998; Stefani and Caputo, 1998). Domal uplift associated with magmatism is reflected by the radial pattern of the Ladinian dykes in the central-western part of the Dolomites (Doglioni, 1983). The orientation of the major axis of the dome (N70E, Stava Line, Cima Bocche anticline, Selle Line) was possibly controlled by a zone of weakness, inherited from previous sinistral transcurrent faults.

6. Analytical methods

More than two hundred rocks have been collected during three fieldwork campaigns from 2015 to 2017. All the samples were cut to produce thin sections and, after a detailed petrographic check, 61 of them were selected for whole-rock chemical analyses (28 lavas from the Dolomites, 19 plutonic and volcanic rocks from Predazzo, 8 plutonic rocks from Monzoni and 6 lavas from the Vicentinian Alps; Fig.

2). Representative samples were cut with a diamond-disc saw to small chips to completely remove weathered parts. These were first crushed in a steel mill to about mm-scale fragments, then washed with distilled water and dried at 110 °C overnight. The dried and clean chips were powdered in a low-blank agate mortar to a size passing 200-mesh sieve.

Whole-rock major and trace element analyses were performed at Activation laboratories (Ontario, Canada) using Code 4LITHO Major Elements Fusion ICPAES and trace Elements Fusion ICPMS. The detection limit ranges from 0.001 to 0.01 % for major elements, 0.1 to 30 ppm for trace element and 0.004 to 0.1 ppm for REE.

Mineral chemistry analyses were performed at the *Istituto di Geologia Ambientale e Geoingegneria* (CNR-IGAG) laboratory, *Dipartimento di Scienze della Terra* of Sapienza University of Rome, with a CAMECA SX50 electron microprobe. The analyses were carried out at 15 kV accelerating voltage, 15 nA beam current, 10 µm beam diameter for feldspar and 1 µm for pyroxene and opaque minerals. Counting times were 20 s at the peak position and 10 s for background for all elements. Calibration was made on synthetic and natural minerals.

Seven representative samples from the volcanic rocks of the Dolomites area have been analysed for Sr-Nd-Pb isotope ratios at the *Istituto di Geoscienze e Georisorse*, (CNR-IGG) in Pisa. Rocks powders ì were dissolved in HF+HNO_3 and then completely dried. Sr and Nd were extracted by ion exchange chromatography. Lead was extracted from the matrix after eluting with HBr and HCl. The separated Sr, Nd and Pb aliquots were loaded on Re filaments and then loaded into a Finnigan Mat 262 multi-collector Thermal Ionization Mass Spectrometer (TIMS). A complete description of the analytical techniques is reported in Di Giuseppe et al. (2017).

7. Results

7.1. Petrographic description and mineral chemical composition

The investigated samples are essentially massive rocks (44 samples; dykes, sills and lava flows) plus rarer pyroclastic facies rocks (4 samples) from the Dolomites. Seven volcanic rocks from Vicentinian Alps (hereafter referred to as Recoaro), 8 plutonic rocks from Monzoni and 16 plutonic rocks from Predazzo complete the dataset. This research focusses on the massive volcanic rocks of the Dolomites and consequentially only minor comments will be devoted to the other volcanic and plutonic rocks presented here, the readers being referred to the recent articles of Casetta et al. (2018a, 2018b) and to Bonadiman et al. (1994) for Predazzo and Monzoni plutonic rocks description, respectively. A detailed petrographic description of the two types of Dolomite volcanic rocks and their mineral chemical compositions is reported in the electronic appendix 1.

7.2. Whole-rock chemistry

Thirty-one representative samples of Dolomites volcanic rocks were analysed for whole-rock chemistry. The results of these chemical analyses and CIPW normative minerals are reported in Table 1. In the same table, new whole-rock analyses of Recoaro volcanic rocks as well as the Monzoni and Predazzo plutonic rocks are reported too. Selected major oxides and trace elements of the new and literature data (a total of 1120 whole-rock analyses, available as Electronic Appendix 3) are reported in Figs. 6 and 7. For sake of clarity, the same diagrams, with each single district shown at the time, are reported in the Electronic Appendix 4.

In terms of silica content, the massive volcanic rocks of the Dolomites are basic to intermediate (SiO_2 = 49.2-58.1 wt%, LOI-free basis) with alkali content (Na_2O+K_2O) ranging from 4.0 to 7.9 wt%. The Loss-on-ignition (LOI) value is generally <3 wt%, although few samples record higher values (up to 7.3 wt%). Based on TAS classification scheme (Le Maitre, 2002), the analysed samples are classified mostly as trachybasalts and basaltic trachyandesites, with minor alkali basalts, basaltic andesites and one trachyandesite (Fig. 3a). The Alpe di Siusi hyaloclastite tuff (sample AS6) is characterised by fresh glassy shards. These show peculiar compositions, being characterised by higher SiO_2 (55.1-64.0 wt%) and alkalis (Na_2O+K_2O = 10.4-13.1 wt%) than the massive rocks. The glassy shard compositions mostly fall in the trachyte field with rarer tephri-phonolite and one trachyandesite (Fig. 3a). Only the altered tuff sample shows a sodic alkaline affinity, falling in the mugearite field, possibly indicating K_2O depletion.

The Monzoni plutonic rocks range from ultrabasic to intermediate compositions (SiO_2 = 41.7-57.2 wt%), aligned along a rather sharp trend with mild enrichment of alkalis ($Na_2O + K_2O$ = 1.6-7.6 wt%). The Predazzo plutonic rocks spread over a much larger range of SiO_2 (44.0-75.9 wt%) and alkalis (Na_2O+K_2O = 1.5-9.6 wt%), completely overlapping the Monzoni rocks, straddling the subalkaline-alkaline division in the TAS diagram, reaching rhyolitic compositions, with a gap in the trachyte field. The Recoaro volcanic rocks mostly fill the Predazzo rock gap, plotting in the 59.3-69.6 wt% SiO_2 range. As already discussed in the literature (De Vecchi and Sedea, 1983), and confirmed in this study, the Recoaro rocks are characterised by strong alkali mobility, rendering handling of geochemical data of these samples at least dubious (see the discussion section).

In the K_2O vs. Na_2O diagram (Fig. 3b), all the Dolomites samples fall into the field of the transitional and potassic series fields, with the exception of two outliers characterised by high LOI. The two outliers are the Lago di Alleghe mugearitic tuff (LOI = 5.8 wt%), characterised by anomalously high Na_2O (6.3 wt% on LOI-free basis) and very high Na_2O/K_2O (3.93), and the Alpe di Siusi shoshonite (LOI = 6.2 wt), which is characterised by high K_2O (5.7 wt%) and low Na_2O/K_2O (0.38). Also in this case, the EMP compositions of sample AS6 glassy shards fall into the potassic and ultrapotassic series fields (Fig. 3b). The new samples from Predazzo, Monzoni and Recoaro districts completely overlap the Dolomites rock field.

According to the K_2O vs. SiO_2 diagram (Peccerillo and Taylor, 1976), most of the investigated rocks belong to the high-K calcalkaline and shoshonitic series, (Fig. 3c), as most of the samples reported in literature. Only moderately to strongly altered SiO_2-rich samples from Vicentinian and Brescian areas tend to plot in the calcalkaline or arc-tholeiite fields, due to K_2O depletion. On the AFM Diagram (Kuno, 1968), all the studied samples and the literature analyses plot in the calcalkaline field, lacking substantial iron enrichment during the evolutionary trend (Fig. 3d).

More than half of the Dolomites samples are SiO_2-saturated with CIPW normative orthopyroxene and olivine. Six are characterised by slight normative quartz content (0.62-4.98%), and eight of them are SiO_2-undersaturated with normative nepheline ranging from 1.92 to 7.42%. The glassy shards in the hyaloclastite sample range from slightly SiO_2-oversaturated (with CIPW normative quartz = 1.7-3.3%) to slightly SiO_2-undersaturated (normative nepheline = 1.1-3.4%). More than 37% of Monzoni samples, more than 60% of the Predazzo samples and all the Recoaro rocks are quartz-normative.

The major oxides of the analysed samples were plotted vs. the Differentiation Index parameter (D.I.= sum of CIPW normative Q, Or, Ab, Ne, Lc and Kp; Thornton and Tuttle, 1960) in Fig. 4. When considering the entire dataset, MgO, TiO_2, Fe_2O_{3tot} and CaO exhibit well defined negative correlation with D.I (Fig. 4). Al_2O_3 and P_2O_5 define bell-shaped patterns, with maximum at ~60 and ~40, respectively, whereas a correlation is observed for SiO_2, K_2O (well-defined) and Na_2O (more scattered) vs. D.I.. The glassy shards usually overlap whole-rock data of the other Triassic igneous rocks from the Alps and Dinarides.

Predazzo plutonic rocks define a large and quite continuous spread of major oxides, showing always a good correlation with D.I., in nearly all the cases with R^2 >0.85 (up to >0.96 for CaO and Fe_2O_{3tot}). Monzoni and Recoaro rocks exhibit straight correlations with D.I. too, overlapping the trend of the previous two areas.

All the Dolomites samples are metaluminous with ASI [ASI = Alumina Saturation Index = Al/(Na+K+Ca)] ranging from 0.52 to 1.00, similarly to what observed for the Alpe di Siusi glassy shards (ASI = 0.75-0.95) and the other investigated Southern Alps igneous rocks. A good correlation exists between ASI and D.I., with ASI values increasing from 0.47 to 1.00 in the 19.2-66.8 D.I. range. Only the most evolved compositions (D.I. >78; SiO_2 >66.5 wt%) have peraluminous compositions with ASI as high as 1.49. Mg number [Mg# = 100*Mg/(Mg+Fe^{2+}), assuming Fe^{3+} = 0.15% ΣFe] of Dolomites rocks ranges from 35 to 63, with no correlation with D.I. and a poor correlation with SiO_2 (R^2 = 0.39, excluding the two SiO_2-richest samples). On the contrary, the Predazzo and Recoaro rocks show good negative correlations of Mg# with SiO_2 (R^2 = 0.96 and 0.86, respectively). The low Mg# value, coupled with relatively low Cr (30-330 ppm) and Ni (20-80 ppm) indicate that the investigated rocks cannot be considered primary melts in equilibrium with mantle rocks and that they experienced fractionation during their ascent to the surface (see below).

Selected trace elements are plotted vs. D.I. in Fig. 5. Dolomites rocks show no correlation between compatible/incompatible elements and D.I.. Light-REE (LREE; La, Ce, Pr, Nd and Sm) are roughly correlated with SiO_2, except for sample PR23 (highly altered basaltic andesite). Middle-REE (MREE: Eu, Gd, Tb, Dy, and Ho) and heavy-REE (HREE; Er, Tm, Yb and Lu) do not show any correlation with D.I..

The other three investigated SATIR districts show recognizable and rather coherent trends. Among LILE, only Rb behaves as an incompatible element, showing enrichment with increasing D.I. (Fig. 5). Strontium and Ba reach a peak at D.I. ~50 and then decrease. Transition elements show well-defined negative trends with D.I., particularly evident for Sc, V and Co (Fig. 5). HFSE + Y behave as a coherent group, aligning along straight correlation with D.I., with the only exception of the most differentiated compositions of Predazzo (D.I. >87). What described for the HFSE is mimicked by the REE, with the exception of Eu, which is strongly depleted in the most differentiated Predazzo samples (Fig. 5). Thorium and U behave as strongly incompatible elements, and the most differentiated Predazzo samples are characterised by high Th (up to 70 ppm) and U (up to 14 ppm). Lead distribution is less defined for all the districts.

Primitive mantle (PM)-normalised multi-elemental patterns (Fig. 6) are similar with limited inter-elemental fractionation for the different analysed rock types. Key features of the patterns are medium to high enrichment of LILE (Rb ~39-315, Ba ~39-143, Th ~38-181, U ~40-168, K ~46-235 and Pb ~42-257 times PM), deep Nb-Ta troughs (~13-26 times PM), strong trough at Ti (~3-8 times PM) and very flat HREE (Ho_N/Lu_N = 1.02-1.29). The Dolomite rocks define a pattern that, with the only exception of P, perfectly overlaps the Global Subducting Sediment (GloSS) composition (Plank, 2014). When compared to a classical within-plate oceanic locality such as the St. Helena basalts in central Atlantic Ocean (the type locality of HiMu-OIB), the Dolomite rocks show remarkable differences, in particular much higher LILE, negative anomalies at Nb-Ta-Ti and strong positive peaks at K and Pb (Fig. 6a).

The rocks from the other three investigated districts (Predazzo and Monzoni plutons and Recoaro) show inter-elemental fractionation patterns similar to those of Dolomites volcanic rocks. The Predazzo plutonic rocks nearly overlap the incompatible elements of Dolomites, showing slightly higher Rb, peaking at U-Th. Predazzo clinopyroxenites show the lowest incompatible element content, but overall they have the same pattern of the bulk plutonic rocks. The only syenitic sample analysed here (PR25) is characterised by the highest enrichment in nearly all the elements (Fig. 6b). Predazzo granites have an even more spiked pattern, with deep troughs at Ba, Sr, P, Eu and Ti and the highest concentration for the other elements, as well as flat HREE clustering around 13-16 PM times (Fig. 6c). Monzoni plutonic rocks closely resemble the Dolomites lava pattern too, sharing strong similarities with the GloSS composition, albeit incompatible elements content is

generally displaced towards lower abundances (Fig. 6d). Also in this case the cumulitic rocks (gabbros) show very low elemental content, overlapping the Predazzo pyroxenites.

The Recoaro samples are usually displaced towards higher incompatible element contents, with the exceptions of deeper troughs at Sr, P and Ti. The sample with the highest LOI (HA9; LOI = 4.19 wt%) slightly depart from the main pattern; in particular it displays the lowest Sr and P and a high MREE-HREE content (Fig. 6e).

7.3. Sr-Nd-Pb isotopic ratios

Based on petrographic characteristics, geochemical signatures and geographic position, seven Dolomites volcanic rock samples were selected for Sr-Nd-Pb isotopic determination. These analyses are reported in Table 2 and shown in Fig. 7, with the isotopic ratios corrected to 238 Ma. The Dolomites samples have relatively high $^{87}Sr/^{86}Sr_{(i)}$ (0.7043-0.7051) with $\varepsilon Sr_{(i)}$ ranging from 1.8 to 12.7, with the exception of a Latemar basaltic dyke (LAT2) that shows slightly more radiogenic $^{87}Sr/^{86}Sr$ (0.7058) with $\varepsilon Sr_{(i)}$ 22.5. The $^{143}Nd/^{144}Nd_{(i)}$ ranges from 0.51227 to 0.51237, with $\varepsilon Nd_{(i)}$ values slightly lower to slightly higher than $ChUR_{(238\ Ma)}$ (from -1.4 to +0.5). The Pb isotopic compositions are homogeneous, with $^{206}Pb/^{204}Pb$ clustered around 18.26 and 18.41, $^{207}Pb/^{204}Pb$ from 15.62 to 15.67 and $^{208}Pb/^{204}Pb$ from 38.36 to 38.48, with the exception of sample LAT2 showing $^{208}Pb/^{204}Pb$=38.89, slightly higher than in the other samples.

The Dolomites lavas mostly plot in the enriched Sr-Nd isotopic quadrant (Fig. 7a), partially overlapping the plutonic rock compositions of Predazzo plutonic rocks (Casetta et al., 2018b), but being displaced towards slightly more radiogenic Nd compared to Monzoni plutonic rocks (Bonadiman et al., 1994) for a given $^{87}Sr/^{86}Sr$. Recent data from Valsugana dykes (poorly age constrained at 227-260 Ma with K/Ar datings; Bianchini et al., 2018), sampled between Dolomites and Vicentinian Alps, ~10-15 km E of Trento city, are characterised by a much larger content of radiogenic Sr ($^{87}Sr/^{86}Sr$ = 0.7082-0.7172) and much lower content of radiogenic Nd ($^{143}Nd/^{144}Nd$ = 0.51197-0.51209; Fig. 7a).

To the best of the authors' knowledge, the only Pb isotopic data on SATIR are those reported for the sulphides in Maso Furli, Val di Non, Doss de la Grave and Sasso Negro areas (Nimis et al., 2012) and for Valsugana dykes (Bianchini et al., 2018). The new data presented here show a partial overlap with these literature data, being the Valsugana dykes characterised by sensibly higher content of radiogenic $^{206}Pb/^{204}Pb$ (18.57-19.12) and $^{207}Pb/^{204}Pb$ (15.68-15.72; Fig. 7b,c). No direct comparison with $^{208}Pb/^{204}Pb$ can be made, because Th elemental content to recalculate the initial values is not reported in Bianchini et al. (2018). Assuming a reasonable Th/Pb ratio ~0.5 for the Valsugana dykes, the $^{208}Pb/^{204}Pb_{(238\ Ma)}$ ratios of these samples ranges from 38.87 to 40.19, values much more radiogenic than those for Dolomites massive rocks presented here.

The Dolomites samples analysed in this study completely overlap the Predazzo and Monzoni plutonic rocks in terms of $^{87}Sr/^{86}Sr$ and do not show any appreciable variation with SiO_2 or MgO, similarly to what recorded by Predazzo and Monzoni plutonic samples (Fig. 7a,b). The Valsugana dykes are displaced towards very high radiogenic values, but again without any correlation with differentiation parameters. On the other hand, the Northern Karawanken (Austria) Triassic igneous rocks mimic increase of $^{87}Sr/^{86}Sr$ with increase of magma evolution. With the exception of the most evolved sample analysed here, no correlation between $^{143}Nd/^{144}Nd$ and SiO_2 or MgO is observed (Fig. 7c,d). The samples analysed here are the most radiogenic among the SATIR in terms of $^{143}Nd/^{144}Nd$, with higher ratios recorded in the Karawanken pluton only (Miller et al., 2011). As Pb isotopes are concerned, the bulk of the Dolomites samples does not show any correlation with SiO_2 or MgO, even if the most evolved sample (PR3 latite; 1.8 wt% MgO) is characterised by the lowest $^{207}Pb/^{204}Pb$ (Fig. 7e,f).

8. Discussion

New and literature data on SATIR are discussed with three approaches, the first focussing on the origin of the inter- and intra-district geochemical variations, the second trying to constrain the composition of mantle source(s) and the third aiming to define a geotectonic model in a large scale geological framework.

8.1. Inter- and intra-district geochemical variations.

As a whole, our data define relatively coherent trends in Harker-type diagrams for SATIR. This is particularly surprising, considering their subaqueous emplacement, with associated variable degrees of element mobility, the large width of the study area (>4000 km^2; Figs. 1 and 2) and the thick and compositionally heterogeneous crust pierced by the various magma batches.

When major elements are plotted against differentiation parameters such as SiO_2, MgO or D.I., some important considerations can be made:

1) Figures 6 and 7 show the major oxide and trace element variation against D.I. for the four investigated districts (Dolomites volcanic rocks, Predazzo and Monzoni plutonic rocks and Recoaro volcanic rocks). With a few exceptions, the investigated rocks define positive (SiO_2, Na_2O+K_2O) and negative correlation (TiO_2, Fe_2O_{3tot}, MnO, MgO, CaO, CaO/Al_2O_3) with D.I. (Fig. 4). Only Al_2O_3 does not show any clear trend with this index, with a rough bell-shaped pattern, being mostly confined in the 14.5-19 wt% range with D.I. ranging from ~5 to ~60.

2) The samples with the lowest and highest D.I. values are plutonic rocks. Among these, the Monzoni samples mostly show poor- to medium-evolved compositions. Predazzo rocks span the largest chemical variation for all the major oxides (e.g., SiO_2 = 40.2-78.3 wt%; MgO = 0.0-11.9 wt%; Alkalis = 0.7-12.0 wt%). The Dolomites

volcanic rocks show a rather restricted compositional range compared to the other SATIR districts.

3) The Monzoni and Predazzo samples with the lowest D.I. show similar compositions, resembling accumulation/fractionation of clinopyroxene (CaO = 15.6-16.2 wt%; Na_2O+K_2O = 1.5-1.6 wt%) and variable accumulation of Fe-Ti oxides (Fe_2O_{3tot} = 14.7-22.9 wt%; TiO_2 = 1.3-1.5 wt%) and minor amounts of intercumulus plagioclase (CaO/Al_2O_3 = 0.9-3.0; Fig. 4), coherently with the interpretation provided in the literature (Bonadiman et al., 1994; Casetta et al., 2018a).

4) In the literature, the Predazzo plutonic rocks have been divided into four (SiO_2-saturated and SiO_2-oversaturated shoshonite, potassic and calcalkaline; Visonà, 1997) or three (SiO_2-saturated shoshonite, SiO_2-undersaturated shoshonite and granitic; Casetta et al., 2018a) groups. However, in the diagrams reported in Electronic Appendix 4 no substantial intra-district differences can be evidenced. With the exception of a small Na_2O enrichment of a restricted sub-group (Casetta et al., 2018a), the remaining Predazzo rocks follow a rather continuous liquid line of descent, with most evolved samples displaying strong SiO_2 and K_2O enrichment, and Al_2O_3 and Na_2O decrease, questioning the actual existence of different serial affinities in this plutonic complex. Our new data are qualitatively consistent with a gabbroic fractionation to explain the gabbro-to-syenite transition (Casetta et al., 2018a). Worth noting, however, none of the hypothetical fractionating assemblages proposed by Casetta et al. (2018a) reflects the composition of the cumulitic clinopyroxenites, characterised by <10% plagioclase.

5) The most differentiated syenogranitic samples of Predazzo are not considered cogenetic with the rest of the plutonic rocks because of the impossibility to model fractional crystallization processes (Casetta et al., 2018a). Consequently, the existence of three distinct magma batches has been proposed in literature (Visonà, 1997; Casetta et al., 2018a). Given the large volume of granitic magma (~1 km^3), its derivation from less differentiated melts via prolonged fractional crystallization is quite improbable. Similar mechanisms perhaps operated during the Permian rift stages in the Oslo rift, where small differences in silica activity of mafic to intermediate melts evolving in variable conditions (pressure, $P_{H2O/CO2}$, fO_2) generated a series of magma chambers at various levels in the thinned continental crust. Relatively hot magma ponding may have caused local crust partial melting generating evolved liquids with D.I. up to 94, with limited genetic link with mafic and intermediate magmas (Neumann, 1980).

6) The Mg# and major oxide variation of Dolomites volcanic rocks suggest fractional crystallization of Mg-bearing phases such as olivine and pyroxene. No quantitative assessment can be made because of the absence of clear correlations of major oxides and trace elements with D.I. The rough correlation of Al_2O_3 vs. D.I. and the strong negative correlation of CaO/Al_2O_3 vs. D.I. of Ladinian volcanic rocks indicate

only a minor role of plagioclase in the fractionating assemblage, despite its common presence among the phenocryst phases and the Eu/Eu* <1 (1.01-0.75).

7) The definition of the serial affinity of SATIR is not as straightforward as it could be assumed. Essentially, all the SATIR plot in the calcalkaline field in the AFM diagram (Fig. 3d). On the other hand, in the Miyashiro (1974) FeO_{tot}/MgO vs. SiO_2 diagram, modified by Arculus (2003), more than two thirds of the SATIR (with <70 wt% SiO_2) show relatively high FeO_{tot}/MgO, clustering in the tholeiitic field (mostly "Medium-Fe field" of Arculus, 2003).

The mildly alkaline composition of most of the SATIR (Fig. 3a), coupled with variable K_2O/Na_2O ratios (mostly in the 0.3-1.6 range; average 1.16 ± 0.58) and the common mobility of alkalis, with widespread leakage of Na_2O and enrichment of K_2O (e.g., De Vecchi and Sedea, 1983), render the definition of the magmatic affinity a difficult task. Despite these caveats, we agree with the common use of "shoshonitic affinity" for the SATIR, whose least differentiated compositions have ~1.2-3.9 wt% K_2O in the MgO 6-8 wt% and SiO_2 49.2-51.2 wt% interval.

7) A limited to moderate amount (2-10 wt%) of assimilation of Permian micaschist/dioritic/rhyolitic/carbonate country rocks can explain the inter-group Sr and Nd isotopic variation of Predazzo plutonic rocks (Casetta et al., 2018a). The $^{143}Nd/^{144}Nd$-$^{87}Sr/^{86}Sr$ correlation of silica-undersaturated shoshonitic group of Predazzo (albeit defined by three samples only) is at odd with a crustal contamination process, but Casetta et al. (2018a) interpreted the spread of Sr isotopic ratios with local fluid mobilization along the intrusion borders.

8) The high Rb/Sr of the most differentiated plutonic rocks of Predazzo does not allow precise recalculation of the initial $^{87}Sr/^{86}Sr$ isotopic ratios (Casetta et al., 2018b). Initial Nd isotopic ratios of Predazzo granites ($^{143}Nd/^{144}Nd$ = 0.51222-0.51230) overlap with those of the less differentiated compositions (0.51219-0.51229). More in detail, on the basis of the differences in Nd isotopes, Casetta et al. (2018b) confirm an earlier hypothesis of the existence of two independent magma batches for the least differentiated rocks with silica-undersaturated ($^{143}Nd/^{144}Nd_i$ = 0.51226-0.51229) and silica-saturated shoshonitic groups (0.51219-0.51225. Our Predazzo granitic rocks have not been analysed for isotopic ratios, but they could be qualitatively interpreted as the most extreme differentiation products of the basic compositions (gabbros). The major oxide variation seen in Fig. 4 indicates the possible involvement of feldspars in the latest crystallization phases, causing an abrupt change in the pattern of Al_2O_3, Na_2O and, less evident, K_2O. The strong depletion of Sr and Ba in the most differentiated samples of Predazzo is compatible with such a process, as well as the strong depletion of Hf and Zr could involve zircon fractionation. In any case, volumetric considerations on the evolved and least differentiated igneous compositions speak against simple direct derivation via fractional crystallization processes.

9) Only a few SATIR samples have been analysed in literature for both Sr-Nd isotopes and whole-rock analyses (5 from Monzoni, 8 from Predazzo, 8 from Karawanken, and 8 from Valsugana). Our seven samples are the first covering the entire Dolomites area. The situation for Pb isotopes is even worst, being the data presented here the first for the entire SATIR, with the exception of the recent work of Bianchini et al. (2018) on Valsugana dykes. Excluding the few Monzoni data (Bonadiman et al., 1994) and two basaltic and andesitic 218 Myr-old lavas from Brescian Alps (Cassinis et al., 2008), all the SATIR plot along a classical hyperbolic trend in $^{143}Nd/^{144}Nd$ vs. $^{87}Sr/^{86}Sr$ diagram (Fig. 8a). This is classically interpreted as the result of interaction of mantle melts with ancient continental crust or the derivation from ancient mantle sources that have experienced variable degrees of melt extractions and/or modifications in the form of digestion of subducted material (e.g., Lustrino et al., 2011; Lustrino and Anderson, 2015, and references therein). In the first case, the isotopic ratios are expected not to vary or to vary without any correlation with evolutionary degrees, while in the case of continental crust clear contamination trends should emerge with major oxides.

$^{87}Sr/^{86}Sr$ ratios of the Dolomites volcanic rocks presented in this study (0.70432-0.70577) do not show any correlation with D.I. (R^2 = 0.03), with SiO_2 (R^2 = 0.001) or MgO (R^2 = 0.14). The spread of isotopic data can be interpreted, therefore, as characteristic of the mantle sources, only little modified by interaction with local crust. Interestingly, Predazzo and Monzoni rocks (with the exception of the SiO_2-richest sample) do not show any correlation with D.I. too (R^2 = 0.02 and 0.0004, respectively). The same conclusions can be obtained for the (fewer) $^{143}Nd/^{144}Nd$ vs. D.I. trends. In conclusion, most of the isotopic variation seen in the SATIR is here related do mantle source heterogeneities rather than to post-melting interaction with upper crustal lithologies. It is also worth of noting, however, that interaction of basaltic melt with distinct crustal rock types (e.g., metapelite-metagreywacke-metacarbonate successions, meta-igneous rocks) can lead to the absence of correlation between isotopic ratios and major oxides.

8.2. Constraints on the mantle source(s)

Magmas generated by subduction-modified mantle sources are usually characterised by strongly fractionated incompatible element concentrations, manifested as peaks at U, K and Pb, troughs at Nb, Ta, Ti and, less marked, at Hf and Zr. Other key features are a general LILE enrichment relative to HFSE in primitive mantle-normalised diagrams (Fig. 6a). The Dolomites lava shows high Ba/Nb (32.8-93.9), low Ce/Pb (1.8-10.4) and low U/Nb (0.11-0.33) coupled with low HFSE (e.g., Nb = 6-12 ppm) with negative Nb/Nb* ratio (0.1-0.35), resembling the typical characteristics of magmas generated by subduction-modified mantle sources (Turner and Langmuir, 2015; Kimura, 2017; Schmidt and Jagoutz, 2017; Zheng and Zhao, 2017).

Several are the geochemical tools to infer derivation from a subduction-modified mantle source, and the Th/Yb vs. Ta/Yb diagram is one of the most widely used. It is based on the behaviour of Ta, which is substantially immobile in the restite during the metamorphic reactions in a titanate-bearing sinking slab, while Th is strongly partitioned into the fluid phase (e.g., Brenan et al., 1994) in focused fluid transfer through mantle wedges (Pirard and Hermann, 2015). Moreover, Ta and other HFSE are forced to remain in the subducting slab where titanates with very high K_d^{HFSE} are easily stabilised (e.g., Foley et al., 2000; Kimura, 2017). The Yb at the denominator is used to buffer the absolute Th and Ta values to the same degree of evolution. In Fig. 9a, the Dolomites samples plot outside of the mantle array, displaced towards high Th/Yb ratios (1.3-4.9) for given Ta/Yb values (0.22-0.45). This can be interpreted as additional evidence for the derivation from subduction-modified mantle sources.

The Dolomites lavas are characterised by Eu/Eu* <1 also in the least differentiated terms. The absence of correlation of this parameter with SiO_2, MgO or D.I. indicates source characteristics that could be ultimately related to the digestion of subduction-related recycling of continental crust material (Eu/Eu* = 0.70; Rudnick and Gao, 2003) in their mantle sources, confirming the previous hypothesis.

A quantitative approach to define the intensive and extensive variables that had a role in the genesis of the middle Triassic volcanic rocks of the Dolomites (and in arc magmas in general) is not possible. Only qualitative or semi-quantitative geochemical modelling can be drafted, hypothesizing fundamental parameters responsible for the chemical composition of mantle wedge partial melts.

The latest release of the Arc Basalt Simulator software (ABS5; Kimura, 2017) was used to infer the conditions of magma genesis, assuming for the Dolomites lava the derivation from a supra-subduction mantle wedge. As input parameters, we hypothesized an original mantle source (pristine mantle wedge) with a depleted mantle composition (Salters et al., 2011), with an additional 0.8% MORB extraction from DMM. Additional assumed paremeters are the P-T path of Solomon subduction zone (#32 in Kimura, 2017), slab-derived flux originating at P = 3 GPa, and a slab surface temperature = 792 °C (calculated by ABS5 on the basis of the selected P and P-T path of subduction zone). The slab liquid is assumed to derive 20% from the 0.3 km thick sedimentary cover, and 80% from 0.3 km thick altered oceanic crust in a reactive porous flow regime (%R slab = 90; Kimura 2017). Without the involvement of zone refining processes, open system partial melting is assumed at P = 2.1 GPa and T = 1280 °C, with 2% slab melting and 1.1% peridotite wedge melting. The calculated slab melt contains 1.9 wt% H_2O and the basaltic melt contains 2.1 wt% H_2O. All these parameters represent reasonable values acting in a subduction system.

The composition of the hypothetical liquid produced, together with the hypothetical DMM source and LAT5 potassic basalt are shown in Fig. 9b. Bearing in mind the highly speculative approach, the model results in a close match between

calculated and target (LAT5) melts The calculated degree of melting of the mantle wedge is low, likely due to the effect of non-primary composition of the target melt (LAT5). Indeed, during fractional crystallization, incompatible elements tend to be concentrated in the residual melts, and this process is modelled by ABS5 reducing the degree of melting. The overlap between the calculated melt and LAT5 sample is nearly total in terms of incompatible element budget, with slight differences only in very mobile elements such as Rb, Th and K. In conclusion, the results obtained with ABS5 software indicate, with the necessary caveats, that it is possible to obtain a basaltic liquid with incompatible element fractionation and absolute content closely resembling that of basalt sample LAT5 assuming typical subduction settings from a peridotitic mantle wedge source.

8.3. *Geodynamic and tectonic setting.*

Although paleotectonic environments are usually inferred interpreting geochemical characters of igneous rocks (e.g., Pearce and Cann, 1973; Meschede, 1986; Saccani, 2015), a warm caveat seems to emerge in recent literature in using tectonic discrimination diagrams (e.g., Li et al., 2015). In particular, it has been suggested that the geochemical signature needs always to be checked against y geological/geophysical data (e.g., Lustrino et al., 2011, 2016). When misfits arise between geochemical data and geological/geophysical evidence, a solution needs to be looked for. Several authors invoked ancient (i.e., not directly related with the coeval tectonic setting) subduction-related modifications of mantle sources to reconcile such misfits (e.g., Lustrino et al., 2011; Mazzeo et al., 2014; Gaeta et al., 2016; Di Giuseppe et al., 2018). In other cases, the geochemical message of igneous rocks has been explained with shallow rather than deep geological processes (i.e., contamination of mantle melts with upper crustal lithologies instead of subduction-modified mantle sources; e.g., Esperança et al., 1992).

The SATIR were emplaced during Pangea rifting in a mainly transtensional tectonic setting, as testified by Triassic tectonic structures widespread in the Southern Alps (Doglioni 1984, 1987; Brandner et al., 2016a, Abbas et al., 2018). However, the geodynamic scenario that originated these tectonic structures is still matter of debate. Indeed, the recorded stratigraphic successions and extensional tectonic structures have been alternatively related to rifting processes of the Meliata-Maliac Ocean (Gawlick et al., 2012; Sudar et al., 2012; Brandner et al., 2016b; Ferriere et al., 2016). Conversely, other paleogeographic settings have been proposed for the Middle Triassic western Tethys, invoking active subduction processes located west (Brack et al., 1999) or south (Stampfli et al., 2013) of Adria, Dinarides and Southern Alps nappes.

In this study we advocate, for the SATIR, an origin from subduction-modified (not directly subduction-related) mantle sources. The existence of a direct volcanic arc settings, as instead proposed by several authors (a.o., Castellarin et al., 1988;

Garzanti 1985; Zanetti et al. 2013; Bianchini et al., 2018) can be excluded because the Rheic Ocean was already completely exhausted in the Alpine realm during Middle Triassic times. A back-arc setting for the SATIR (e.g., Marinelli et al. 1980; Viel, 1982; Brack et al., 1999; Cassinis et al., 2008) can be similarly excluded, because of geochemical considerations on Eisenkappel magmatism (Northern Karawanken, eastern Alps), pointing to anorogenic magmatism in an extensional setting (e.g., Visonà and Zanferrari, 2000; Miller et al., 2011).

Back-arc basins are characterised by progressive migration of extensional tectonics and magmatism. Typical examples of migrating magmatism are described for the Tyrrhenian Sea, associated with the Apennine subduction (Carminati et al., 2012), for the Lau Basin, associated with the Tonga subduction (e.g., Hawkins, 1995) and for the Parece Vela Basin, associated with the Marianas subduction (Ishizuka et al., 2010). The existence of a Middle Triassic back-arc basin setting is in our view unlikely because of two major observations: 1) the SATIR activity does not show any age-space migration trend of magmatism, differently from what observed in present-day back-arc basins. Indeed, the oldest SATIR occurred in the central-eastern part of the 450 km wide volcanic area, and subsequent activity occurred to the east and to the west with no clear trends (Fig. 1); 2) Magmas generated in back-arc basins have both MORB and subduction affinities, differently from the SATIR case (Taylor and Martinez, 2003).

The disagreement between the geochemical message of the igneous rocks (i.e., derivation from mantle sources modified by subduction) and the geological evidence (i.e., development of continental rift with horst-and-graben structures) requires a specific solution. The most likely model in this case is the derivation of partial melts by mantle sources previously modified by the north-directed subduction of the Rheic oceanic lithosphere before the late Carboniferous Gondwana-Laurussia collision.

9. Conclusions

During Middle-Late Triassic time, a large area in the Southern Alps experienced an intense and diffuse igneous activity. This magmatism (here referred to as SATIR = Southern Alps Triassic Igneous Rocks) followed the Devonian-Carboniferous subduction of the Rheic Ocean and the Carboniferous collision between the northern margin of Gondwana and the southern sectors of Laurussia with the development of Pangea. The last subduction stages and the collisional events were associated with abundant Permian calcalkaline to potassic magmatism in large sectors of the Variscan/Hercynian Chain.

During early Mesozoic, the Southern Alps portion of Pangea was affected by extensional tectonics with formation of intra-montane rifts and the development of horst-and-graben structures. This extensional tectonic phase ultimately evolved into the development, in Middle Triassic time, of huge carbonate platforms along subsiding area. During a narrow (<1 Myr) eruptive interval (Storck et al., 2019) huge

amounts of magmas reached the surface in Southern Alps, now represented by volcaniclastic and epiclastic deposits up to 150 m thick, massive lava flows, dyke swarms and rare plutonic complexes.

The igneous products are characterised by a wide compositional spectrum with compositions ranging from metaluminous basalt/gabbros to peraluminous rhyolites/leucogranites, including also cumulitic lithologies such as ultrabasic clinopyroxenites. The petrography, mineral chemistry, whole-rock chemistry and Sr-Nd-Pb isotopic ratios point to the derivation of the least differentiated melts from a subduction-modified mantle source. The shoshonitic affinities defined in terms of K_2O vs. SiO_2 are the most abundant, followed by high-K calcalkaline types. The mildly to strongly evolved compositions are generically linked with the least differentiated terms by closed system fractional crystallization of gabbroic to monzonitic assemblages, even if the SiO_2-richest magmas likely require a separate origin.

At a large scale, no substantial differences can be recorded in the four districts investigated in this study (Dolomites lavas, Predazzo, Monzoni and Vicentinian Alps), all sharing similar geochemical affinity and likely similar mantle sources, identified in a depleted mantle metasomatised by subduction event(s). A close geochemical modelling and quantification of evolutionary processes is hindered by the bad preservation state of some of the samples (e.g., the Vicentinian Alps) and, in general, by the absence of true primitive magmas and the abundance of mildly to strongly evolved compositions.

The geochemical message of these products, that is derivation from a subduction-modified mantle source, is at odds with the geological, sedimentological and structural evidence indicating that magmatism occurred in association with tectonic and geodynamic processes (rifting and/or wrench tectonics) that will eventually lead to the development of the Adria passive margins. The apparent paradox can be solved requiring the activation of upper mantle sources, contaminated during the previous Variscan subduction, when local geotherms were raised due to the passive upwelling of asthenospheric mantle along the rifted margins.

10. Acknowledgements

H.A. thanks the Erasmus Mundus European Commission for providing financial support for 33 months in framework of EU METALIC II project (Erasmus Mundus Action 2) during his PhD program. This article benefitted of thorough and detailed reviews of Tom Andersen (Oslo, Norway), Stefan Jung (Hamburg, Germany), Jörn-Frederik Wotzlaw (Zurich, Switzerland) and an anonymous reviewer. To all of them our thanks for the work that helped to clarify many aspects of the article. We thank also the Editor Sebastian Tappe (Johannesburg, South Africa) for coordinating the review process and for precious hints to improve the text readability. Special thanks to Marcello Serracino (CNR-IGAG, Rome) for his assistance during the electron microprobe analyses, to Domenico Mannetta for his help during the thin section

production and to Paolo Di Giuseppe for his assistance during the isotope analyses. Funding by FAR 2016-2017 (M. Caggiati and P. Gianolla) and Progetti di Ateneo 2016 and 2017 (E. Carminati and M. Lustrino) is acknowledged. M.L. indifferently thanks Sergio Bruni.

References

Abbas, H., Michail, M., Cifelli, F., Mattei, M., Gianolla, P., Lustrino, M., Carminati, E., 2018. Emplacement modes of the Ladinian plutonic rocks of the Dolomites: insights from anisotropy of magnetic susceptibility. J. Struct. Geol., 113, 42-61.

Arculus, R.J., 2003. Use and abuse of the terms calcalkaline and calcalkalic. J. Petrol., 44, 929-935.

Armienti, P., Corazzato, C., Groppelli, G., Natoli, E., Pasquarè, G., 2003. Geological and petrographical study of Montecampione Triassic subvolcanic bodies (Southern Alps, Italy): preliminary geodynamic results. Boll. Soc. Geol. It. Spec., 2, 67-78.

Avanzini, M., Bargossi, G.M., Borsato, A., Castiglioni, G.B., Cucato, M., Morelli, C., Prosser, G., Sapelza, A., 2007. Note Illustrative - Foglio 026 Appiano, Carta Geol. It. 1:50000: Roma, ISPRA, p. 184.

Barbieri, G., De Vecchi, Gp., De Zanche, V., Mietto, P., Sedea, R., 1982. Stratigrafia e petrologia del magmatismo triassico di Recoaro. In: A. Castellarin e G.B. Vai (Eds.), Guida alla geologia del Sudalpino centro-orientale. Guide Geol. Reg. Soc. Geol. It., 179-187.

Beccaluva, L., Coltorti, M., Saccani, E., Siena, F., Zeda, O., 2005. Triassic magmatism and Jurassic ophiolites at the margins of the Adria Plate. In: I.R. Finetti (Ed.) CROP PROJECT: Deep seismic exploration of the central Mediterranean and Italy. Elsevier, 607-618.

Bechstadt, T., Brandner, R., Mostler, H., Schmidt, K., 1977. Aborted rifting in the Triassic of the Eastern and Southern Alps. N. Jb. Geol. Palaont. Abh., 156, 157-178.

Bell, T.H., Newman, R., 2006. Appalachian orogenesis: the role of repeated gravitational collapse. Geol. Soc. Am. Spec. Paper, 414, 95-118.

Bellieni, G., Fioretti, A.M., Marzoli, A., Visonà, D., 2010. Permo–Paleogene magmatism in the eastern Alps. Rend. Lincei, 21, 51-71.

Beltrán-Triviño, A., Winkler, W., von Quadt, A., Gallhofer, D., 2016. Triassic magmatism on the transition from Variscan to Alpine cycles: evidence from U-Pb, Hf, and geochemistry of detrital minerals. Swiss J. Geosci., 109, 309-328.

Bertotti, G., Picotti, V., Bernoulli, D., Castellarin, A., 1993. From rifting to drifting: tectonic evolution of the South-Alpine upper crust from the Triassic to the Early Cretaceous. Sedim. Geol., 86, 53-76.

Bianchini, G., Natali, C., Shibata, T., Yoshikawa, M., 2018. Basic dykes crosscutting the crystalline basement of Valsugana (Italy): new evidence of early Triassic volcanism in the Southern Alps. Tectonics, 37.

Blendinger, W., 1985. Middle Triassic strike-slip tectonics and igneous activity of the Dolomites (Southern Alps). Tectonophysics, 113, 105-121.

Bonadiman, C., Coltorti, M., Siena, F., 1994. Petrogenesis and T-fO_2 estimates of Mt. Monzoni complex (Central Dolomites, Southern Alps): a Triassic shoshonitic intrusion in a transcurrent geodynamic setting. Eur. J. Mineral., 6, 943-966.

Boriani, A., Caironi, V., Giobbi Origoni, E., Vannucci, R., 1992. The Permian intrusive rocks of Serie dei Laghi (Western Southern Alps). Acta Vulcanol., 2, 73-86.

Bosellini, A., Castellarin, A., Doglioni, C., Guy, F., Lucch NI, F., Perri, M.C., Rossi, P.I., Simboli, G., Sommavill, E., 1982. Magmatismo e tettonica nel Trias delle Dolomiti. In: Castellarin, A. and Vai, G.B. (Eds.) Guida alla Geologia del Sudalpino centro-orientale. Soc. Geol. It., 189-210.

Bosellini, A., Gianolla P., Stefani M., 2003. Geology of the Dolomites. Episodes, 26, 181-185.

Bosellini, A., Hardie, L.A., 1973. Depositional theme of a marginal marine evaporite. Sedimentol., 20, 5-27.

Brack, P., Mundil, R., Oberli, F., Meier, M., Rieber, H., 1997. Biostratigraphic and radiometric age data question the Milankovitch characteristics of the Latemar cycles (Southern Alps, Italy). Reply. Geology, 25, 471-472.

Brack, P., Muttoni, G., 2000. High-resolution magnetostratigraphic and lithostratigraphic correlations in Middle Triassic pelagic carbonates from the Dolomites (northern Italy). Palaeogeogr. Palaeoclimatol. Palaeoecol. 161, 361-380.

Brack, P., Rieber, H., 1993, Towards a better definition of the Anisian/Ladinian boundary: new biostratigraphic data and correlations of boundary sections from the Southern Alps. Heclog. Geol. Helv., 86, 415-527.Brack, P., Rieber, H., Mundil, R., Blendinger, W., Maurer, F., 2007. Geometry and chronology of growth and drowning of Middle Triassic carbonate platforms (Cernera and Bivera/Clapsavon) in the Southern Alps (northern Italy). Swiss J. Geosci., 100, 327-348.

Brack, P., Rieber, H., Nicora, A., Mundil, R., 2005. The Global boundary Stratotype Section and Point (GSSP) of the Ladinian Stage (Middle Triassic) at Bagolino (Southern Alps, Northern Italy) and its implications for the Triassic time scale. Episodes, 28, 233-244.

Braid, J.A., Murphy, J.B., Quesada, C., Gladney, E.R., Dupuis, N., 2018. Progressive magmatism and evolution of the Variscan suture in southern Iberia. Int. J. Earth Sci., 107, 971-983.

Brandner, R., 1984. Meeresspiegelschwankungen und Tektonik in der Trias der NW Tethys. Jb. Geol., 126, 435-475.

Brandner, R., Gruber, A., Morelli, C., Mair, V., 2016. Pulses of Neotethys-Rifting in the Permomesozoic of the Dolomites. Geo. Alp., 13, 7-70.

Brandner, R., Keim, L., 2011. A 4-day geological field trip in the Western Dolomites. Geo. Alp., 8, 76-118.

Brenan, J.M., Shaw, H.F., Phinney, D.L., Ryerson, F.J., 1994. Rutile-aqueous fluid partitioning on Nb, Ta, Hf, Zr, U and Th: implications for the high field strength element depletions in island-arc basalts. Earth Planet. Sci. Lett., 128, 327-339.

Brusca, C., Gaetani, M., Jadoul, F., Viel, G., 1982. Paleogeografia Ladino-Carnica e metallogenesi nel Sudalpino. Mem. Soc. Geol. It., 22, 65-82.

Buser, S., 1980. Tolmač za list Celovec (Klagenfurt). Osnovna geološka karta SFRJ 1:100.000: Beograd, Zvezni Geol. Zavod, p. 62.

Buser, S., 1986. Tolmač za list Tolmin in Videm (Udine). Osnovna geološka karta SFRJ 1:100.000: Beograd, Zvezni Geol. Zavod, p. 103.

Calanchi, N., Lucchini, F., Rossi, P.L., 1978. The volcanic rocks from the Mount Agnello area (Fiemme Valley, Italy): a contribution to the knowledge of the Mid-triassic magmatism of the Southern Alps. Tsch. Mineral. Petrol. Mitt., 25, 131-143.

Caputo, R., Poli, M. E., Zanferrari, A., 2010. Neogene–Quaternary tectonic stratigraphy of the eastern Southern Alps, NE Italy. J. Struct. Geol., 32, 1009-1027.

Carminati, E., Doglioni, C., 2012. Alps vs. Apennines: the paradigm of a tectonically asymmetric Earth. Earth-Sci. Rev., 112, 67-96.

Carminati, E., Lustrino, M., Doglioni, C., 2012. Geodynamic evolution of the central and western Mediterranean: Tectonics vs. igneous petrology constraints. Tectonophysics, 579, 173-192.

Casetta, F., Coltorti, M., Ickert, R.B., Bonadiman, C., Giacomoni, P.P., Ntaflos, T., 2018b. Intrusion of shoshonitic magmas at shallow crustal depth: T-P path, H_2O estimates, and AFC modeling of the Middle Triassic Predazzo Intrusive Complex (Southern Alps, Italy). Contrib. Mineral. Petrol., 173, 57.

Casetta, F., Coltorti, M., Marocchino, E., 2018a. Petrological evolution of the Middle Triassic Predazzo Intrusive Complex, Italian Alps. Int. Geol. Rev., 60, 977-997.

Cassinis G., Corbari D., Falletti P., Perotti C., 2011. Note Illustrative della Carta Geologica d'Italia alla scala 1:50.000; Foglio 099 Iseo. ISPRA, Litografia Artistica Cartografica S.R.L., 246 pp., Firenze.

Cassinis, G., Cortesogno, L., Gaggero, L., Perotti, C.R., Buzzi, L., 2008. Permian to Triassic geodynamic and magmatic evolution of the Brescian Prealps (eastern Lombardy, Italy). Boll. Soc. Geol. It., 127, 501-518.

Cassinis, G., Zezza, U., 1982. Dati geologici e petrografi ci sui prodotti del magmatismo triassico nelle Prealpi Bresciane. In: Castellarin A. and Vai G.B. (Eds.), Guida alla geologia del Sudalpino centro-orientale. Guide Geol. Reg. Soc. Geol. It., 157-171.

Castellarin, A., Lucchini, F., Rossi, P.L., Sartori, R., Simboli, G., Sommavilla E., 1982. Note geologiche sulle intrusioni di Predazzo e dei M. Monzoni. In Castellarin A. &

Vai G.B. (Eds.): Guida alla geologia del Sudalpino centro-orientale. Guide Geol. Reg. Soc. Geol. It., 213-219.

Castellarin, A., Lucchini, F., Rossi, P. L., Selli, L., Simboli, G., 1988. The Middle Triassic magmatic-tectonic arc development in the Southern Alps. Tectonophysics 146, 79-89.

Castellarin, A., Pisa, G., 1973. Le vulcaniti Ladiniche di Forni di Sopra (carnia occidentale). Mem. Museo Trident. Sc. Nat., 20, 99-136.

Castellarin, A., Selli, L., Picotti, V., Cantelli, L., 1998. Tettonismo e diapirismo Medio-Triassico delle Dolomiti. Mem. Soc. Geol. It., 53, 145-169.

Castellarin, A., Vai, G.B., Cantelli, L., 2006. The Alpine evolution of the Southern Alps around the Giudicarie faults: A Late Cretaceous to Early Eocene transfer zone. Tectonophysics, 414, 203-223.

Celarc, B., Gorican, S., Kolar-Jurkovšek, T., 2013. Middle Triassic carbonate-platform break-up and formation of small-scale half-grabens (Julian and Kamnik–Savinja Alps, Slovenia). Facies, 9, 583-610.

Cocherie, A., Rossi, Ph., Fouillac, A.M., Vidal, Ph., 1994. Crust and mantle contributions to granite genesis – An example from the Variscan batholith of Corsica, France, studied by trace-elements and Sr-Nd-O isotope systematics. Chem. Geol., 115, 173-211.

Cortesogno, L., Cassinis, G., Dallagiovanna, G., Gaggero, L., Oggiano, G., Ronchi, A., Seno, S., Vanossi, M., 1998. The Variscan post-collisional volcanism in Late Carboniferous-Permian sequences in Ligurian Alps, Southern Alps and Sardinia (Italy): a synthesis. Lithos, 45, 305-328.

Crisci, C.M., Ferrara, G., Mazzuoli, R., Rossi, P.M., 1984. Geochemical and geochronological data on Triassic volcanism of the Southern Alps of Lombardy (Italy): genetic implications. Geol. Rund., 73, 279-292.

Cros, P., 1980. Relations paleogeographiques entre la sedimentation tufacee et les apports terrigenes, Trias Moyen et Superieur des Dolomites et des Alpes Carniques. Riv. It. Paleont. Strat., 85, 953-982.

Davidson J.P., 1996. Deciphering mantle and crustal signatures in subduction zone magmatism. In: Bebout, G.E., Scholl, D.W., Kirbyand, S.H., and Platt, J.P. (Eds.) Subduction Top to Bottom. Washington, D.C., American Geophysical Union, 251-262.

De Vecchi, G., Sedea, R., 1983. Il vulcanismo medio-triassico nelle Prealpi vicentine (Italia settentrionale). Mem. Sci. Geol., 36, 14-169.

De Vecchi, G., Sedea, R., Di Lallo, E., 1986. Note illustrative della carta geologica dell'area di Valli del Pasubio-Posina-Laghi: alla scala 1: 20.000. Mem. Sci. Geol. 38, 187-205.

De Zanche, V., Gianolla, P., Mietto, P., Siorpaes, C., Vail, P.R., 1993. Triassic sequence stratigraphy in the Dolomites (Italy). Mem. Sci. Geol., 45, 1-27.

Di Giuseppe, P., Agostini, S., Lustrino, M., Karaoglu, O., Savasçin, M.Y., Manetti, P., Ersoy, Y., 2017. Transition from compression to strike-slip tectonics revealed by Miocene-Pleistocene volcanism west of the Karliova Triple Junction (East Anatolia). J. Petrol., 58, 2055-2087.

Di Giuseppe, P., Agostini, S., Manetti, P., Savasçin, M.Y., Conticelli, S., 2018. Sub-lithospheric origin of Na-alkaline and calc-alkaline magmas in a post-collisional tectonic regime: Sr-Nd-Pb isotopes in recent monogenetic volcanism of Cappadocia, Central Turkey. Lithos, 316, 304-322.

Doglioni, C., 1983. Duomo medio-triassico nelle Dolomiti. Rend. Soc. Geol. It., 6, 13-16.

Doglioni, C., 1984. Triassic diapiric structures in the central Dolomites (Northern Italy). Ecl, Geol. Helv., 77, 261-285.

Doglioni, C., 1987. Tectonics of the Dolomites (Southern Alps, Northern Italy). J. Struct. Geol., 9, 181-193.

Doglioni, C., 1988. Examples of strike-slip tectonics on platform-basin margins. Tectonophysics, 156, 293-302.

Doglioni, C., 1992. Relationships between Mesozoic extensional tectonics, stratigraphy and Alpine inversion in the Southern Alps. Eclog. Geol. Helv., 85, 105-126.

Doglioni, C., Carminati E., 2008. Structural styles and Dolomites Field Trip. Mem. Mem. Descr. Carta Geol. It., 82, 296 pp.

Dozet, S., Buser, S., 2009. Triassic, in Pleničar, M., Ogorelec, B., and Novak, M., eds., The geology of Slovenia: Lubiana, Geološki Zavod Slovenije, 161-214.

Esperança, S., Crisci, G.M., de Rosa, R., Mazzuoli, R., 1992. The role of the crust in the magmatic evolution of the island of Lipari (Aeolian Islands, Italy). Contrib. Mineral. Petrol., 112, 450-462.

Fan, W.M., Guo, F., Wang, Y. J., Lin, G., 2003. Late Mesozoic calc-alkaline volcanism of post-orogenic extension in the northern Da Hinggan Mountains, northeastern China. J. Volcanol. Geotherm. Res., 121, 115-135.

Foley, S.F., Barth, M.G., Jenner, G.A., 2000. Rutile/melt partition coefficients for trace elements and an assessment of the influence of rutile on trace element characteristics of subduction zone magmas. Geochim. Cosmochim. Acta, 64, 933-938.

Fondriest, M., Smith, S.A.F., Di Toro, G., Zampieri, D., Mittempergher, S., 2012. Fault zone structure and seismic slip localization in dolostones, an example from the Southern Alps, Italy, J. Struct. Geol., 45, p. 52-67.

Franke, W., Cocks, L.R.M., Torsvik, T.H., 2017. The Paleozoic Variscan oceans revisited. Gondw. Res., 48, 257-284.

Gaeta, M., Freda, C., Marra, F., Arienzo, I., Gozzi, F., Jicha, B., Di Rocco, T., 2016. Paleozoic metasomatism at the origin of Mediterranean ultrapotassic magmas:

constraints from time-dependent geochemistry of Colli Albani volcanic products (Central Italy). Lithos, 244, 151-164.

Gaggero, L., Gretter, N., Langone, A., Ronchi, A., 2017. U-Pb geochronology and geochemistry of late Palaeozoic volcanism in Sardinia (southern Variscides). Geosci. Front., 8, 1263-1284.

Garzanti, E., 1985. The sandstone memory of the evolution of a Triassic volcanic arc in the Southern Alps, Italy. Sedimentol., 32, 423-433.

Gianolla, P., 1992. Evoluzione mediotriassica del vulcanismo di Rio Freddo (Alpi Giulie, Italia). Mem. Sci. Geol., 44, 193-209.

Gianolla, P., Avanzini, M., Breda, A., Kustatscher, E., Preto, N., Roghi, G., Furin, S., Massari, F., Picotti, V., Stefani, M., 2010. Field trip to the world heritage site of the Tethysian Triassic, September 5-10, 2010, Dolomites, Southern Alps, Italy. 122 pp.

Gianolla, P., De Zanche, V., Mietto, P., 1998. Triassic Sequence Stratigraphy in the Southern Alps. Definition of sequences and basin evolution. In: P.C. de Graciansky, J. Hardenbol, T. Jacquin, P.R. Vail and D. Ulmer-Scholle (Eds.): Mesozoic-Cenozoic Sequence Stratigraphy of European Basins, SEPM Special Publication 60, 723-751, Tulsa/Oklahoma.

Gianolla, P., Morelli, C., Cucato, M., Siorpaes, C. 2018. Note Illustrative della Carta Geologica d'Italia alla scala 1:50.000, Foglio 016, Dobbiaco. ISPRA, Systemcart, 283 pp., Roma.

Gianolla, P., Neri, C., 2007. Formazione di Wengen. In: Cita Sironi, M.B., Abbate, E., Balini, M., Conti, M.A., Falorni, P., Germani, D., Groppelli, G., Manetti, P., Petti, F.M. (Eds.): Carta Geologica d'Italia 1:50.000, Catalogo delle Formazioni-Unità tradizionali (2), QUADERNI serie III, 7/VIII. S.E.L.CA, Firenze, 111-124.

Handy, M.R., Schmid, S.M., Bousquet, R., Kissling, E., Bernoulli, D., 2010. Reconciling plate-tectonic reconstructions of Alpine Tethys with the geological–geophysical record of spreading and subduction in the Alps. Earth-Sci. Rev., 102, 121-158.

Hart, S.R., 1984. A large-scale isotope anomaly in the Southern Hemisphere mantle. Nature, 309, 753-757.

Hawkins, J.W., 1995. The geology of the Lau Basin. In: Back arc Basins, 63-138, Springer, Boston, MA.

Ishizuka, O., Yuasa, M., Tamura, Y., Shukuno, H., Stern, R. J., Naka, J., Joshima, M., Taylor, R.N., 2010. Migrating shoshonitic magmatism tracks Izu–Bonin–Mariana intra-oceanic arc rift propagation. Earth Planet. Sci. Lett., 294, 111-122.

Jadoul, F., Galli, M.T., Berra, F., Cirilli, S., Ronchi, P., Paganoni, A., 2004, The Late Triassic-Early Jurassic of the Lombardy Basin: Stratigraphy, Palaeogeography and Palaeontology, 32nd IGC Florence August 20-28 2004, Excursion Guide book, Volume 68, 36 pp.

Keim, L., Brandner, R., Krystyn, L., Mette, W., 2001. Termination of carbonate slope progradation: an example from the Carnian of the Dolomites, Northern Italy. Sedim. Geol., 143, 303-323.

Kimura, J.I., 2017. Modeling chemical geodynamics of subduction zones using the Arc Basalt Simulator version 5. Geosphere, 13, 992-1025.

Kroner, U., Romer, R.L., 2013. Two plates – many subduction zones: the Variscan orogeny revisited. Gondw. Res., 24, 298-329.

Kuno, H., 1968. Differentiation of basalt magmas. Intersci., 2, 623-688.

Kustatscher, E., Bernardi, M., Petti, F.M., Franz, M., van Konijnenburg-van Cittert, J.H.A., Kerp, H., 2017. Sea-level changes in the Lopingian (late Permian) of the northwestern Tethys and their effects on the terrestrial palaeoenvironments, biota and fossil preservation: Glob. Planet. Change, 148, 166-180.

Lan, T. G., Fan, H. R., Santosh, M., Hu, F. F., Yang, K. F., Yang, Y. H., Liu, Y., 2012. Early Jurassic high-K calc-alkaline and shoshonitic rocks from the Tongshi intrusive complex, eastern North China Craton: implication for crust–mantle interaction and post-collisional magmatism. Lithos, 140, 183-199.

Le Maitre, R.W. (Ed.), 2002. Igneous rocks. A Classification of Igneous Rocks and Glossary of Terms. Cambridge Univ. Press., New York, 236 pp.

Li, C., Arndt, N.T., Tang, Q., Ripley, E.M., 2015. Trace element indiscrimination diagrams. Lithos, 232, 76-83.

Liegeois, J. P., Navez, J., Hertogen, J., Black, R., 1998. Contrasting origin of post-collisional high-K calc-alkaline and shoshonitic versus alkaline and peralkaline granitoids. The use of sliding normalization. Lithos, 45, 1-28.

Lucchini, F., Rossi P.L., Simboli, G., Viel, G., 1980. Dati petrochimici ed inquadramento stratigrafico della serie vulcanica medio-triassica dell'area di Tarvisio (Carnia). Miner. Petr. Acta, 24, 135-150.

Lucchini, F., Rossi, P.L., Simboli G., 1982. Il magmatismo triassico dell'area di Predazzo (Alpi Meridionali, Italia). In: A. Castellarin and G.B. Vai (Eds.), Guida alla geologia del Sudalpino centro-orientale. Guide Geol. Reg. Soc. Geol. It., 221-230.

Lustrino, M., Anderson, D.L., 2015. The mantle isotopic printer: Basic mantle plume geochemistry for seismologists and geodynamicists. Geol. Soc. Am. Spec. Paper, 514, 257-279.

Lustrino, M., Duggen, S., Rosenberg, C.L., 2011. The Central-Western Mediterranean: anomalous igneous activity in an anomalous collisional tectonic setting. Earth-Sci. Rev., 104, 1-40.

Lustrino, M., Prelevic, D., Agostini, S., Gaeta, M., Di Rocco, T., Stagno, V., Capizzi, L.S., 2016. Ca-rich carbonates associated with ultrabasic-ultramafic melts: Carbonatite or limestone xenoliths? A case study from the late Miocene Morron de Villamayor volcano (Calatrava volcanic field, central Spain). Geochim. Cosmochim. Acta, 185, 477-497.

Lyubetskaya, K., Korenaga, J., 2007. Chemical composition of Earth's primitive mantle and its variance. Methods and results. J. Geophys. Res., 112, doi:10.1029/2005JB004223.

Macera, P., Del Moro, A., Bargossi, G.M., Campana, R., Rottura, A., 1994. Polygenetic nature of the Cima d'Asta intrusive complex, Southern Alps, Italy. Inferences from petrological, geochemical and isotopic (Sr and Nd) data. Lithos, 32, 47-62.

Marinelli, M., Viel, G., Farabegoli, E., 1980. Il Permo-Trias delle Alpi Meridionali: evoluzione tardo-ercinica di un bacino marginale di retroarco sialico. Ind. Min., 6, 1-14.

Marocchi, M., Morelli, C., Mair, V., Klötzli, U., Bargossi, G.M., 2008. Evolution of Large Silicic Magma Systems: New U-Pb Zircon Data on the NW Permian Athesian Volcanic Group (Southern Alps, Italy). J. Geol., 116, 480-498.

Maron, M., Muttoni, G., Rigo, M., Gianolla, P., Kent, D.V., 2019 New magnetobiostratigraphic results from the Ladinian of the Dolomites and implications for the Triassic geomagnetic polarity timescale. Palaeog. Palaeoclim. Palaeoec., 517, 52-73.

Masetti, D., Trombetta, G.L., 1998. L'eredità anisica nella nascita ed evoluzione delle piattaforme medio-triassiche delle dolomiti occidentali: Mem. Sci. Geol., 50, 213-237.

Massari, F., Neri, C., 1997. The infill of a supradetachment (?) basin: the continental to shallow-marine Upper Permian succession in the Dolomites and Carnia (Italy). Sedim. Geol., 110, 181-221.

Maurer, F., 2000, Growth mode of Middle Triassic carbonate platforms in the Western Dolomites (Southern Alps, Italy). Sedim. Geol., 134, 275-286.

Maurer, F., Schlager, W., 2003. Lateral variations in sediment composition and bedding in Middle Triassic interplatform basins (Buchenstein Formation, southern Alps, Italy). Sedimentol., 50, 1-22.

Mazzeo, F.C., D'Antonio, M., Arienzo, I., Aulinas, M., Di Renzo, V., Gimeno, D., 2014. Subduction-related enrichment of the Neapolitan volcanoes (Southern Italy) mantle source: new constraints on the characteristics of the slab-derived components. Chem. Geol., 386, 165-183.

Meschede, M., 1986. A method of discriminating between different types of mid-ocean ridge basalts and continental tholeiites with the Nb-Zr-Y diagram. Chem. Geol., 56, 207-218.

Mietto, P., Manfrin, S., Preto, N., Rigo, M., Roghi, G., Furin, S., Gianolla, P., Posenato, R., Muttoni, G., Nicora, A., Buratti, N., 2012. The global boundary stratotype section and point (GSSP) of the Carnian stage (Late Triassic) at Prati di Stuores/Stuores Wiesen section (Southern Alps, NE Italy). Episodes, 35, 414-430.

Miller, C., Thoni, M., Goessler, W., Tessadri, R., 2011. Origin and age of the Eisenkappel gabbro to granite suite (Caringhia, SE Austrian Alps). Lithos, 125, 343-448.

Miyashiro, A., 1974. Volcanic rock series in island arcs and active continental margins. Am. J. Sci., 274, 321-355.

Moghazi, A.M., 2003. Geochemistry and petrogenesis of a high-K calc-alkaline Dokhan Volcanic suite, South Safaga area, Egypt: the role of late Neoproterozoic crustal extension. Precambr. Res., 125, 161-178.

Mundil, R., Brack, P., Meier, M., Rieber, H., Oberli, F., 1996. High resolution U-Pb dating of Middle Triassic volcaniclastics: Time scale calibration and verification of tuning parameters for carbonate sedimentation. Earth Planet. Sci. Lett., 141, 137-151.

Neri, C., Gianolla, P., Furlanis, S., Caputo, R., Bosellini, A., 2007. Note Illustrative della Carta Geologica d'Italia alla scala 1:50.000, Foglio 029 Cortina d'Ampezzo. Roma: Systemcart, 200 pp.

Neumann, E.-R., 1980. Petrogenesis of the Oslo Region larvikites and associated rocks. J. Petrol., 21, 499-531.

Neumann, E.-R., Wilson, M., Heeremans, M., Spence, E.A., Obst, K., Timmerman, M.J., Kirstein, L., 2004. Carboniferous-Permian rifting and magmatism in southern Scandinavia, the North Sea and northern Germany: a review. Geol. Soc. London Spec. Publ., 223, 11-40.

Nimis, P., Omenetto, P., Giunti, I., Artioli, G., Angelini, I., 2012. Lead isotope systematics in hydrothermal sulphide deposits from the central-eastern Southalpine (northern Italy). Eur. J. Mineral., 24, 23-37.

Obenholzner, J.H., Pfeiffer, J., 1991. “Pietra verde" - ein Diskussionsbeitrag zur Geodynamik der Südalpen: Jubiläumsschrift 20 Jahre Geologische Zusammenarbeit Österreich - Ungarn, 1, 221-245.

Pamic, J.J., 1984. Triassic magmatism of the Dinarides in Yugoslavia: Tectonophysics, 109, 273-307.

Pearce, J.A., 1982. Trace element characteristics of lavas from destructive plate boundaries. In: Thorpe R.S. (Ed.) Andesites, 8, 525-548, John Wiley & Sons.

Pearce, J.A., Cann, J.R., 1973. Tectonic setting of basic volcanic rocks determined using trace element analyses. Earth Planet. Sci. Lett., 19, 290-300.

Pearce, J.A., Peate, D.W., 1995. Tectonic implications of the composition of volcanic arc magmas. Annu. Rev. Earth Planet Sci., 23, 251-285.

Peccerillo, A., Taylor, S.R., 1976. Geochemistry of Eocene calc-alkaline volcanic rocks from the Kastamonu area, northern Turkey. Contrib. Mineral. Petrol., 58, 63-81.

Perini, G., Cebrià, J.M., Lopez-Ruiz, J., Doblas, M., 2004. Carboniferous-Permian magmatism in the Variscan Belt of Spain and France: implications for mantle sources. Geol. Soc. London Spec. Publ., 223, 415-438.

Pinarelli, L., Del Moro, A., Boriani, A., Caironi, V., 2002. Sr, Nd isotope evidence for an enriched mantle component in the origins of the Hercynian gabbro-granite series of the “Serie dei Laghi” (Southern Alps, NW Italy). Eur. J. Mineral., 14, 403-415.

Pirard, C., Hermann, J., 2015. Focused fluid transfer through the mantle above subduction zones. Geology, 43, 915-918.

Pisa G., Castellarin A., Lucchini F., Rossi P.L., Simboli G., Bosellini A., Sommavilla E., 1980. Middle Triassic magmatism in Southern Alps. I: a review of general data in the Dolomites. Riv. It. Paleont. Strat., 85, 1093-1110.

Plank, T., 2014. The chemical composition of subducting sediments. Treat. Geochem., 4, 607-629.

Preto, N., Spötl, C., Mietto, P., Gianolla, P., Riva, A., Manfrin, S., 2005. Aragonite dissolution, sedimentation rates and carbon isotopes in deep-water hemipelagites (Livinallongo Formation, Middle Triassic, northern Italy). Sedim. Geol., 181, 173-194.

Quick, J.E., Sinigoi, S., Peressini, G., Demarchi, G., Wooden, J.L., Sbisà, A., 2009. Magmatic plumbing of a large Permian caldera exposed to a depth of 25 km. Geology, 37, 603-606.

Romer, R.L., Forster, H.-J., Breitkreuz, C., 2001. Intracontinental extensional magmatism with a subduction fingerprint: the late Carboniferous Halle Volcanic Complex (Germany). Contrib. Mineral. Petrol., 141, 201-221.

Rossi, D., 1973. II conglomerato di Richthofen e la superficie di discordanza alla sua base: Atti Acc. Roveretana Agiati Sci., Lett. Arti, 13, 3-20.

Rossi, P.L., Morten, L., Petersen, J.S., 1980. The Middle Triassic volcanic rocks from Non Valley, North Italy. Riv. It. Paleont. Strat., 85, 1081-1092.

Rottura, A., Bargossi, G.M., Caggianelli, A., Del Moro, A., Visonà, D., Tranne, C.A., 1998. Origin and significance of the Permian high-K calc-alkaline magmatism in the central-eastern Southern Alps, Italy. Lithos, 45, 329-348.

Rottura, A., Del Moro, A., Caggianelli, A., Bargossi, G.M., Gasparotto, G., 1997. Petrogenesis of the Monte Croce granitoids in the context of Permian magmatism in the Southern Alps, Italy. Eur. J. Mineral., 9, 1293-1310.

Rudnick, R.L., Gao, S., 2003. Composition of the continental crust. In: Rudnick R.L. (Ed.) Treatise on Geochemistry, 1-64.

Saccani, E., 2015. A new method of discriminating different types of post-Archean ophiolitic basalts and their tectonic significance using Th-Nb and Ce-Dy-Yb systematics. Geosci. Front., 6, 481-501.

Sacerdoti, M., Sommavilla, E., 1962. Pillowlave, Ialoclastiti e altre formazioni vulcanoclastiche nella Regione Dolomitica Occidentale. Studi Trent. Sc. Nat., 39, 423-473.

Salters, V.M., Mallick, S., Hart, S.R., Langmuir, C.H., Stracke, A., 2011. Domains of depleted mantle: new evidence from hafnium and neodymium isotopes. Geochem. Geophys. Geosyst., 12, doi:10.1029/2011GC003617.

Schaltegger, U., Brack, P., 2007. Crustal-scale magmatic systems during intracontinental strike-slip tectonics: U, Pb and Hf isotopic constraints from Permian magmatic rocks of the Southern Alps. Int. J. Earth Sci., 96, 1131–1151.

Schmidt, M.W., Jagoutz, O., 2017. The global systematics of primitive arc melts. Geochem. Geophys. Geosyst., 18, 2817-2854.

Sloman, L.E., 1989. Triassic shoshonites from the dolomites, northern Italy: Alkaline arc rocks in a strike-slip setting. J. Geophys. Res., 94, 4655-4666.

Spadea P., 1970. Le ignimbriti riolitiche del membro superiore delle Vulcaniti di Rio Freddo nel Trias medio della regione di Tarvisio (Alpi Giulie Occidentali). St. Trentini Sc. Nat., 47, 287 - 358.

Stahle, V., Frenzel, G., Hess, J. C., Saupé, F., Schmidt, S. T., Schneider, W., 2001. Permian metabasalt and Triassic alkaline dykes in the northern Ivrea zone: clues to the post-Variscan geodynamic evolution of the Southern Alps. Schweiz. Mineral. Petrogr. Mitt., 81, 1-21.

Stefani, M., Furin, S., Gianolla, P., 2010. The changing climate framework and depositional dynamics of Triassic carbonate platforms from the Dolomites. Palaeogeogr. Palaeoclimat. Palaeoecol., 290, 43-57.

Stefani, M., Caputo, R., 1998. Stratigrafia triassica e tettonica alpina nel Gruppo Marmolada-Costabella (Dolomiti centrali). Mem.Soc. Geol. It., 53, 263-293.

Storck, J.-C., Brack, P., Wotzlaw J.-F., Ulmer P., 2019. Timing and evolution of Middle Triassic magmatism in the Southern Alps (Northern Italy). J. Geol. Soc., doi: 10.1144/jgs2018-123.

Sun, S.S., McDonough, W.F., 1989. Chemical and isotopic systematics of oceanic basalts: implication for mantle composition and processes. In: Saunder, A.D. and Norry, M.J. (Eds.), Magmatism in the Ocean Basins. Geol. Soc. Spec. Publ., 42, 313-345.

Taylor, B., Martinez, F., 2003. Back-arc basin basalt systematics. Earth Planet. Sci. Lett., 210, 481-497.

Turner, S., Arnaud, N., Liu, J., Rogers, N., Hawkesworth, G., Harris, N., Deng, W., 1996. Post-collision, shoshonitic volcanism on the Tibetan Plateau: implications for convective thinning of the lithosphere and the source of ocean island basalts. J. Petrol., 37, 45-72.

Turner, S., Langmuir, C.H., 2015. What processes control the chemical compositions of arc front stratovolcanoes? Geochem. Geophys. Geosyst., 16, 1865-1893.

Vardabasso, S., 1930. Carta geologica del territorio eruttivo di Predazzo e Monzoni: ufficio Idrografico del Magistrato alle Acque di Venezia. 1:25,000 2 sheet.

Venturini, C., 2006. Evoluzione geologica delle Alpi Carniche: Udine, Museo Friulano di Storia Naturale, 208 pp.

Viel, G., 1979. Litostratigrafia ladinica: una revisione. Ricostruzione paleogeografica e paleostrutturale dell'area Dolomitica-Cadorina (Alpi Meridionali). Riv. It. Paleont. Strat., 85, 85-125, 297-352.

Viel, G., 1982. Polarità tettonica e vulcanismo ladino-carnici del Sudalpino. Rend. Soc. Geol. It., 261-262, Roma.

Visonà, D., 1997. The Predazzo multipulse intrusive body (Western Dolomites, Italy). Field and mineralogical studies. Mem. Sci. Geol. Univ. Padova, 49, 117-125.

Visonà, D., Zanferrari, A., 2000. Some constraints on geochemical features in the Triassic mantle of the easternmost Australpine-Southalpine domain: evidence from the Karawanken pluton (Carinthia, Austria). Int. J. Earth Sci., 89, 40-51.

Willcock, M.A.W., Bargossi, G.M., Weinberg, R.F., Gasparotto, G., Cas, R.A.F., Giordano, G., Marocchi, M.A., 2015. complex magma reservoir system for a large volume intra- to extra-caldera ignimbrite: mineralogical and chemical architecture of the VEI8, Permian Ora ignimbrite (Italy). J. Volcanol. Geotherm. Res., 306, 17-40.

Wilson, M., Neumann, E.-R., Davies, G.R., Timmermann, M.J., Heeremans, M., Larsen, B.T. (Eds.), 2004. Permo-Carboniferous Magmatism and rifting in Europe. Geol. Soc. London Spec. Publ., 223, 487 pp.

Wotzlaw, J.-F., Brack, P., Storck, J.-C., 2017. High-resolution stratigraphy and zircon U–Pb geochronology of the Middle Triassic Buchenstein Formation (Dolomites, northern Italy): precession-forcing of hemipelagic carbonate sedimentation and calibration of the Anisian–Ladinian boundary interval, J. Geol. Soc., 175, 71-85.

Zanetti, A., Mazzucchelli, M., Sinigoi, S., Giovanardi, T., Peressini, G., Fanning, M., 2013. SHRIMP U-Pb Zircon Triassic Intrusion Age of the Finero Mafic Complex (Ivrea-Verbano Zone, Western Alps) and its geodynamic implications. J. Petrol., 54, 2235-2265.

Zheng, Y-F., Zhao, Z.-F., 2017. Introduction to the structures and processes of subduction zones. J. Asian Earth Sci., 145, 1-15.

Figure captions:

Fig. 1. Geographic (A) and geological (B) setting of the investigated area, with the distribution of volcanic products and possible extension of relative magmatic areas. Numbers in the circles indicate different regions of the Southern Alps: 1) Brescian Prealps; 2) Non Valley and Western Adige Valley; 3) Vicentinian Prealps; 4) Dolomites and Western Carnia; 5) Eastern Carnia and Western Julian Alps; 6) Eastern Julian Alps and Slovenian (Tolmin) Basin; 7) Southern Karawanken and Kamnik-Savinja Alps. PAL: Periadriatic Line; VS: Valsugana Fault System.

Fig. 2. Sampling sites (yellow stars) collected from volcanic (purple) and plutonic (red) outcrops in the Dolomites (a) and in the Vicentinian Alps (b). The regional position of the two regions is reported in Fig. 1. Samples outside the coloured areas are from not mappable outcrops (mainly dykes). Detailed geographic sample locations are reported in Table 1.

Fig. 3. a) Total alkali vs. SiO_2 (TAS) diagram (Le Maitre, 2002) for the studied rocks and literature SATIR (Southern Alps Triassic Igneous Rocks). b) K_2O vs. Na_2O diagram defining the limit between the sodic series and the potassic series among the alkaline rocks. c) K_2O vs. SiO_2 classification (Peccerillo and Taylor, 1976) d) AFM (A = Na_2O+K_2O; F = FeO_{tot}; M = MgO) ternary diagram with boundary curves dividing calc-alkaline and tholeiitic fields (Kuno, 1968). The full list of sources for SATIR is reported in the Electronic Appendix 3.

Fig. 4. Major oxides vs. D.I. for the studied samples and literature SATIR. The full list of sources for SATIR is reported in the Electronic Appendix 3.

Fig. 5. Trace elements vs. D.I. for the studied samples and literature SATIR. The full list of sources for SATIR is reported in the Electronic Appendix 3.

Fig. 6. Primitive mantle-normalised diagrams (normalizing factor after Lyubetskaya and Korenaga, 2007) for the studied rocks. (a) = Dolomites lava; (b) = Predazzo plutonic rocks; (c) = Predazzo granite; (d) Monzoni plutonic rocks. Dotted lines: cumulitic gabbro; (e) = Vicentinian Alps (Schio-Recoaro area). Light blue field in (a) = St. Helena Island basalts (Southern Atlantic Ocean), considered the classical HiMu-OIB composition. Black line = GloSS composition (Global Subducting Sediments; Plank 2014).

Fig. 7. (a) $^{87}Sr/^{86}Sr$ vs. SiO_2; (b) $^{87}Sr/^{86}Sr$ vs. MgO; (c) $^{143}Nd/^{144}Nd$ vs. SiO_2; (d) $^{143}Nd/^{144}Nd$ vs. MgO; (e) $^{207}Pb/^{204}Pb$ vs. SiO_2; (f) $^{207}Pb/^{204}Pb$ vs. MgO of the investigated samples and literature SATIR. The full list of sources for SATIR is reported in the Electronic Appendix 3.

Fig. 8. (a) $^{143}Nd/^{144}Nd$ vs.$^{87}Sr/^{86}Sr$ diagram. (b) $^{208}Pb/^{204}Pb$ vs. $^{206}Pb/^{204}Pb$ diagram. (c) $^{207}Pb/^{204}Pb$ vs. $^{206}Pb/^{204}Pb$ diagram. BSE = Bulk Silicate Earth at 230 Ma; ChUR = Chondritic Uniform Reservoir at 230 Ma. Empty circles and rectangles indicate the

isotopic signatures of the principal mantle sources. DMM, Depleted MORB Mantle; EM-I, Enriched Mantle I; EM-II, Enriched Mantle II; EAR, European Asthenospheric Reservoir; PreMa, Prevalent Mantle. NHRL = Northern Hemisphere Reference Line (Hart, 1984).

Fig. 9. a) Th/Yb vs. Ta/Yb (Pearce, 1982; Pearce and Peate, 1995) diagram for the studied rocks. N-MORB (normal MORB), E-MORB (enriched MORB) and OIB fields are from Sun and McDonough (1989). GloSS, Global Subducted Sediments (Plank, 2014); UCC, Upper Continental Crust. (b) Primitive mantle-normalised diagrams for three compositions: LAT5 represents the most primitive basalt from Dolomites (this study); ABS5 represents the best-fit composition obtained using Arc Basalt Simulator 5 (Kimura, 2017); PERID = Composition of the pre-metasomatism mantle wedge calculated by Arc Basalt Simulator software. The close match between sample LAT5 and the hypothetical melt composition (ABS5) indicates the possibility of derivation of Dolomites magmas from a subduction-modified mantle source. Full details reported in the manuscript.

Table captions:

Table 1. Major and trace-element contents of the studied samples from Dolomites and Vicentinian Alps.

Table 2. Sr-Nd-Pb radiogenic isotope values of representative samples.

Sample label	Area	Locality	Latitude	Longitude	Rock Type	SiO_2	TiO_2	Al_2O_3	Fe_2O_3	MnO	MgO	CaO	Na_2O	K_2O	P_2O_5	L.O.I.	Total	Mg#	Rb	Sr	Ba	Cs	Sc	V	Cr	Co	Ni	Cu	Zn	Y	Zr	Nb	Hf	Ta	La	Ce	Pr	Nd	Sm	Eu	Gd	Tb	Dy	Ho	Er	Tm	Yb	Lu	Pb	Th	U
BEL1	Dolomites	Belvedere	46°26'38.00"N	12°0'4.00"E	Subalkali Basalt	47.66	1.34	17.81	9.98	0.19	5.78	9.02	2.62	1.98	0.40	2.90	99.68	0.57	50	699	376	0.9	25	251	110	33	50	90	100	22	153	8	3.2	1	24.4	52.9	6.65	27.7	6	1.79	5.3	0.8	4.4	0.8	2.4	0.32	2.2	0.33	11	4.2	1
GAR	Dolo	Cima	46°	11°	Suba	50.1	0.87	14.1	9.48	0.21	6.74	11.5	3.10	1.06	0.32	2.30	99.9	0.62	18	596	222		35	248	330	39	70	90	110	19	110	6	2.6	0.9	24.3	50.4	5.99	25.4	5.6	1.43	5	0.8	4.4	0.8	2.3	0.34	2	0.31	8	6.4	1.5

3	mites	Pape, Val di Gares	18'16.00"N	53'9.10"E	lkaliBasalt	8		8				1					5																																		
BUF2	Dolomites	Val Giumela, Buf	46°26'23.00"N	11°44'5.90"E	SubalkaliBasalt	50.36	0.93	14.60	11.09	0.17	5.26	10.78	2.06	1.81	0.34	1.80	99.20	0.52	34	794	466	1.3	30	252	100	38	30	120	100	21	130	9	2.9	0.6	26.9	54.6	6.69	27.2	6.1	1.6	5.1	0.7	4.3	0.8	2.3	0.34	2.1	0.35	12	6.2	1.5

		faure																																																	
AS2	Dolomites	Alpe di Siusi	46°31'38.00"N	11°35'44.00"E	K-Alkali Basalt	49.44	0.91	14.04	12.85	0.20	5.44	10.42	2.05	2.61	0.36	2.15	100.47	0.49	74	758	448	0.6	36	302	90	42	30	120	120	20	118	7	3	0.5	25.7	53.1	6.63	27.3	6	1.67	5.3	0.8	4.2	0.8	2.4	0.32	2.1	0.33	15	6.5	1.8
PR20	Dolomites	Val di S. Nico	46°25'8.20	11°43'38.9	K-Alkali Basa	48.66	1.14	16.44	10.55	0.19	5.27	9.77	2.44	1.93	0.34	2.60	99.32	0.53	51	657	351		29	286	90	35	50	100	110	18	113	7	2.7	0.6	21.1	44.4	5.69	24.4	5.7	1.62	5	0.7	4.1	0.8	2.3	0.29	2.1	0.31	8	3.8	1.1

		lo	"N	0"E	lt																																														
LAT2	Dolomites	Latemar	46°21'2.00"N	11°33'27.00"E	K-Alkali Basalt	48.83	1.31	17.78	10.32	0.20	5.68	9.13	2.73	1.75	0.37	2.34	100.44	0.55	50	830	432	3.7	25	258	100	30	60	90	90	21	148	9	3.2	0.5	22.4	46.8	5.89	24.8	5.3	1.67	4.8	0.7	4	0.8	2.4	0.32	2.1	0.33	7	3.5	1
LAT5	Dolomites	Latemar	46°21'36.00"	11°33'33.00"	K-Alkali Basalt	48.33	1.17	16.65	9.13	0.13	6.30	8.61	2.33	2.23	0.37	3.73	98.98	0.61	53	674	443		27	264	180	29	80	90	90	19	136	9	3.1	0.5	22.7	46.8	5.88	23.8	5.1	1.54	4.5	0.6	3.8	0.7	2.1	0.3	1.8	0.28	6	4.4	1.2

			N	E																																																
BUF4	Dolomites	Val Giumela, Buffaure	46°26'7.00"N	11°42'30.80"E	Potassic Trachybasalt	50.03	0.12	17.44	11.16	0.16	4.08	9.55	2.61	2.43	0.41	1.44	100.44	0.45	58	781	501	0.5	21	261	80	32	30	130	110	22	150	9	3.4	0.6	28.6	59	7.26	30.2	6.5	1.79	5.8	0.8	4.6	0.9	2.5	0.35	2.4	0.34	12	5.9	1.5
AS7	Dolomites	Alpe di Siusi	46°32'2.0	11°34'60.	Potassic Tra	48.61	0.90	15.06	11.47	0.16	7.46	6.69	1.85	3.75	0.38	4.41	100.75	0.59	51	537	726		30	283	70	41	20	120	110	23	125	8	3	0.5	26.7	56	6.99	28.8	6.3	1.65	5.5	0.8	4.7	0.9	2.4	0.34	2.1	0.33	8	6.9	2.1

		si	0"N	00"E	chybasalt																																														
AS8	Dolomites	Alpe di Siusi	46°31'30.00"N	11°34'55.00"E	Potassic Trachybasalt	49.32	0.89	15.20	11.86	0.13	5.69	8.43	2.23	3.00	0.40	2.98	100.13	0.52	73	752	509		29	273	60	37		140	110	21	127	8	3	0.5	27.6	57.5	7.04	29.1	6.3	1.68	5.6	0.8	4.4	0.8	2.3	0.35	2	0.34	8	7.3	2.2
MAR1	Dolo	Marm	46°	11°	Pota	48.0	1.12	18.7	10.3	0.14	4.50	7.69	3.06	2.33	0.46	2.79	99.2	0.49	31	904	598	0.8	18	249	100	36	40	80	130	24	165	11	3.6	0.6	30.1	62.9	7.67	30.6	6.5	1.9	5.6	0.8	4.5	0.9	2.4	0.35	2.2	0.34	10	8.3	2

	mites	olada	27'19.00"N	53'33.00"E	ssicTrachybasalt	5		4	3								1																																
BUL2	Dolomites	Bulla	46°32'58.80"N	11°37'55.20"E	PotassicTrachybas	48.86	0.87	14.69	12.00	0.19	5.83	8.27	2.77	3.22	0.38	2.90	99.99	0.52	65	1091	534	31	272	80	41	30	130	120	22	120	6	2.8	0.9	26.4	55.9	6.81	28.1	6.2	1.59	5.5	0.8	4.5	0.9	2.3	0.32	2.2	0.33	29	6.6	1.7

GAR 1	Dolomites	Cima Pape, Val di Gares	46°18'16.00"N	11°53'9.10"E	alt Potassic Trachybasalt	47.97	1.26	17.09	9.63	0.14	6.30	7.57	3.46	2.11	0.37	3.80	99.70	0.60	41	510	377	2.2	26	243	80	30	40	70	90	22	154	8	3.4	0.9	21.5	46.7	5.81	25.6	5.2	1.63	5.1	0.7	4.4	0.9	2.3	0.35	2.1	0.31	21	3.2	0.9
PR 28	Dolomite	Lago di A	46°24'6	12°1'1.	Mugearite	49.10	1.17	16.79	9.38	0.17	4.79	4.95	5.94	1.51	0.45	5.76	99.99	0.53	28	398	470	7	19	189	30	27		50	100	24	166	11	3.8	0.9	31	63.4	7.5	31.2	6.2	1.82	5.9	0.8	4.8	0.9	2.4	0.36	2.4	0.37		5	1.2

	s	lleghe	.00"N	60"E	c(Tuff)																																														
MAR2	Dolomites	Marmolada	46°27'6.00"N	11°54'14.00"E	Shoshonite	51.06	1.08	19.28	8.03	0.11	2.93	8.19	3.39	2.99	0.42	2.60	100.08	0.45	69	923	554		15	219	70	22	80	180	240	24	147	10	3.6	0.6	32.7	64.9	7.74	30	6	1.78	5.2	0.7	4.4	0.9	2.5	0.35	2.2	0.35	18	7.6	2.2
BUF1	Dolomites	Val Giumela	46°26'26.	11°44'32.	Shoshonite	52.18	0.83	16.52	10.57	0.17	3.17	8.41	2.58	3.19	0.45	1.45	99.52	0.40	80	961	589	0.9	17	185		32		140	120	23	153	9	3.4	0.7	34.1	68.3	8.35	33.4	7.1	1.81	6	0.8	4.6	0.9	2.5	0.36	2.4	0.37	37	8.5	2.3

BUF3PR	Dolomites Do	, Buffaure Val Giumela, Buffaure Fo	20"N 46°26'11.30"N 4	70"E 11°42'57.00"E 1	Shoshonite Sh	51.1251	1.061.	17.7518	9.608.	0.160.	2.332.	9.648.	2.652.	2.642.	0.480.	2.032.	99.4610	0.350.	5964	88388	54153	0.	1815	22819	30	2822	30	14014	11010	2421	16315	1011	3.53.	0.70.	31.731	64.464	7.98.	32.431	6.96.	1.871.	65.	0.80.	4.64.	0.90.	2.52.	0.370.	2.42.	0.360.	1311	6.56.	1.71.

17	lomites	rno, Fiemme valley	6°21'15.00"N	1°37'59.70"E	oshonite	.48	02	.37	88	14	94	75	67	68	44	63	0.00	43		5	7	8		5				0	0		4		6	8	.8	.8	01	.9	7	88	6	8	8	9	5	34	3	37		9	7
AS1	Dolomites	Alpe di Siusi	46°31'30.00"N	11°35'29.00"E	Shoshonite	47.50	0.82	15.30	10.64	0.10	7.97	4.21	2.06	5.41	0.37	6.18	100.60	0.63	112	371	586	1.4	26	239	60	36	20	170	120	21	151	10	3.4	0.9	31.1	64.3	7.59	30.7	6.7	1.75	6.3	0.8	4.5	0.9	2.5	0.34	2.1	0.34	12	7.6	1.9

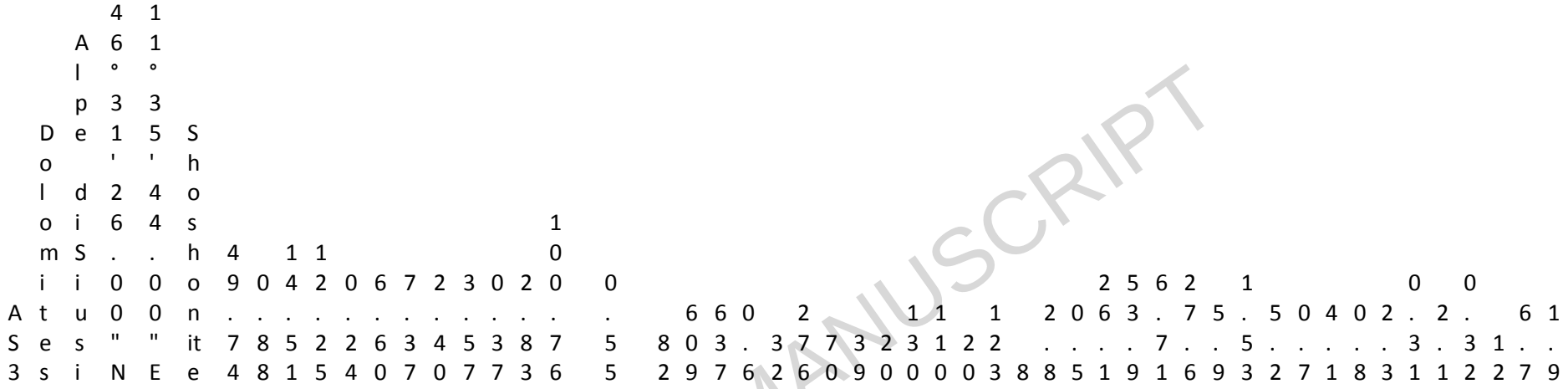

R l l 6 1 o . 8 . . 1 5 6 4 9 3 3 . 5 5 5 7 9 0 0 0 8 1 9 . . 1 . 1 6 3 8 5 8 4 3 2 3 6
o d ° ° s 5 1 2 0 1 1 7 6 2 8 1 0 5 6 1 6 9 1 3 3
2 m i 2 3 h 5 6 6 4
i D 9 9 o
t u ' ' n
e r 3 5 it
s o 3 8 e
n . .
5 2
4 8
" "
N E

4 1
6 1
° °
V 2 4
D a 9 0 S
o l ' ' h
l d 3 3 o
D o i 8 3 s
U m D . . h 5 1 1 9
R i u 3 9 o 1 0 5 0 0 4 9 2 3 0 1 9 0 2 6 7 3 1 0 0
t r 0 0 n . . . . 8 5 2 1 1 1 2 0 8 0 . 0 6 . 5 0 4 0 2 . 2 . 7
3 e o " " it 1 8 2 9 1 5 6 4 0 4 3 7 4 6 7 2 2 3 8 3 2 2 2 2 3 . . . . 3 . . 6 . . . . . 3 . 3 1 .
s n N E e 3 1 2 2 9 9 2 8 5 0 0 2 9 7 2 9 8 0 0 9 0 0 0 1 0 7 9 9 8 7 4 1 4 1 6 8 4 9 4 4 3 2 9 6 2
D D V S 5 0 1 1 0 4 9 2 3 0 1 1 0 2 5 7 2 1 0 0
U o a 4 1 h 0 . 5 1 . . . . 0 . 8 5 0 2 1 1 1 2 0 8 9 . 9 6 . 5 0 4 0 2 . 2 . 7
R l l 6 1 o . 8 . . 1 6 7 5 0 4 2 0 4 7 9 2 . 2 3 8 3 2 2 2 2 2 . . . . 3 . . 6 . . . . . 3 . 3 2 .
o d ° ° s 9 3 5 2 9 0 2 1 6 1 1 . 8 0 1 6 6 8 4 0 9 0 0 0 1 6 6 9 9 7 9 9 4 4 4 6 8 7 9 5 6 2 2 0 5 2

4 m i 2 4 h 3 1 1 2
i D 9 0 o 0
t u ' ' n
e r 3 4 it
s o 8 1 e
n . .
9 4
3 4
" "
N E
4 1
A 6 1
l ° °
p 2 3
D e 9 8 S
o ' ' h
l d 4 3 o
T o i 8 9 s
I m T . . h 5 1 1 9
R i i 7 7 o 2 0 5 6 0 4 0 2 3 0 3 9 0 3 6 7 3 0 0
t r 0 0 n . . . . 9 6 2 1 1 3 3 7 . 2 6 1 5 0 4 0 2 . 2 . 7 2
1 e e " " it 4 8 9 3 1 0 1 5 3 4 2 5 5 6 1 5 2 3 9 2 2 9 2 3 . . . 9 . . . . 3 . 3 1 . .
s s N E e 3 2 7 4 3 3 6 4 8 9 7 6 9 8 1 7 9 7 0 7 0 0 2 4 7 2 1 6 6 3 8 7 7 7 8 7 9 3 5 3 3 3 9 2
T D A S 1
I o l 4 1 h 5 1 1 0
R l p 6 1 o 1 0 5 1 0 4 9 2 3 0 1 0 0 2 5 7 2 1 0 0
o e ° ° s . . . . 8 5 0 2 1 1 1 2 0 8 9 . 9 6 . 5 0 4 0 2 . 2 . 7
2 m 2 3 h 4 8 5 0 1 6 7 4 0 4 3 7 4 6 7 2 . 2 3 9 3 2 2 2 2 2 . . . . 3 . . 5 . . . . . 3 . 3 1 .
i d 9 8 o 8 2 0 9 6 4 6 6 5 1 2 0 8 8 2 0 6 9 2 0 9 0 0 0 1 9 7 9 9 5 4 1 9 2 9 6 8 5 9 5 4 1 5 7 3 2

	tes	iTires	'59.60"N	'58.70"E	nite																																														
LAT3	Dolomites	Latemar	46°20'51.00"N	11°33'28.00"E	Shoshonite	51.78	1.14	19.47	7.35	0.11	2.88	7.78	3.91	3.22	0.40	2.49	100.50	0.47	77	1087	490	5.3	17	219	30	17	20	50	50	24	201	11	3.8	0.9	29.3	62.2	7.35	30.2	6.6	1.64	6.2	0.8	4.7	0.9	2.6	0.37	2.4	0.35	6	5.3	1.3
CIA1	Dolomite	Ciampedi	46°25'5	11°39'3	Shoshonit	49.33	0.85	14.73	9.23	0.16	3.25	9.58	2.21	3.57	0.33	7.28	100.50	0.44	88	599	487	1.7	34	252	180	28	30	110	100	25	125	8	3.3	0.8	31.1	64.4	7.6	31.4	7.3	1.79	6.5	0.9	4.9	0.9	2.6	0.38	2.4	0.34	17	7.5	1.9

	tes	iezzena, Predazzo	'36.00"N	'55.00"E	candesite																																										
PR3	Dolomites	Val Gardonè, Pre	46°19'56.60"N	11°35'21.40"E	Latite	57.08	0.52	19.41	6.04	0.19	1.77	5.04	3.18	4.65	0.37	1.95	100.20	0.40	144	879	707	14.9	9	66	13	20	120	25	177	11	4.1	0.9	39	77.7	9.13	35.3	6.9	1.76	5.5	0.8	4.4	0.9	2.5	0.35	2.3	0.37	24	11.3	2.9

	s	Predazzo	6.30"N	1.40"E	bro																																														
PR8	Dolomites	Predazzo	46°18'52.70"N	11°35'44.50"E	Diorite	48.04	1.11	17.24	11.45	0.19	5.10	8.55	2.78	1.65	0.47	2.46	99.04	0.50	86	906	282	13.2	22	259	40	32	30	70	90	18	108	8	2.7	0.6	29.2	60.2	7.47	31.1	6.7	1.88	5.6	0.8	4.5	0.9	2.4	0.34	2	0.34	19	5.3	1.2
PR15	Dolomite	ValDeser	46°18'4	11°37'4	Monzodio	56.09	0.97	16.70	9.08	0.17	3.28	6.47	2.95	3.24	0.38	0.96	100.29	0.45	124	756	594	7.7	17	175		22		40	110	25	195	12	4.8	1	38.7	77.6	9.32	37	7.5	1.75	6.4	1	5.2	1.1	2.9	0.43	2.8	0.46	22	9.8	2.4

	s	ta, Predazzo	6.00"N	0.90"E	rite																																														
PR13	Dolomites	Predazzo	46°18'23.60"N	11°36'9.10"E	Monzodiorite	58.32	0.76	17.91	6.49	0.15	2.21	4.50	3.57	4.41	0.26	1.44	100.00	0.43	155	741	670	8.2	12	118	30	15	40	100	24	240	16	5.7	1.2	40.8	82.3	9.34	35.7	7	1.73	5.7	0.8	4.7	0.9	2.5	0.4	2.7	0.4	29	12.2	2.8
PR14	Dolom	Preda	46°1	11°3	Monzo	52.91	0.89	15.75	11.16	0.19	3.96	8.31	2.68	3.14	0.38	0.73	100.1	0.44	105	712	462	3.7	24	219	30	34	90	110	23	141	11	3.3	0.8	35.6	72.1	8.88	35	7.4	1.72	6.3	0.9	4.9	1	2.7	0.38	2.4	0.38	18	8.7	1.9

	ites	zzo	9'53.00"N	6'15.10"E	nite												0																																	
PR16	Dolomites	Predazzo	46°18'38.10"N	11°37'59.50"E	Monzonite	53.83	0.82	16.31	9.95	0.19	3.57	7.67	3.13	3.43	0.45	1.41	100.46	0.45	110	925	756	2.9	19	174	50	29	120	120	23	108	11	3	0.8	40	80.4	9.59	38.8	7.9	1.89	6.4	0.9	5.2	1	2.7	0.41	2.6	0.39	34	9.7	1.6
PR25	Dolomit	Predazz	46°18'	11°39'	Monzonit	56.28	0.59	20.53	4.64	0.17	1.22	6.38	5.50	3.05	0.28	1.76	100.40	0.37	113	1316	897	27.8	3	76		5		120	26	234	20	4.6	1.5	97	185	18.4	61.2	9.2	2.69	6.5	0.9	4.8	1	2.9	0.44	2.9	0.45	37	28.4	5.9

	es	o	52.00"N	26.00"E	etoSyenite																																										
LAT1	Dolomites	Predazzo	46°19'41.00"N	11°36'19.00"E	Albitized granite	74.43	0.07	13.25	1.50	0.02	0.15	1.25	2.97	5.43	0.02	1.44	100.54	0.18	372	22	31	6.4	1	70	5	60	178	33	6.2	3.7	54	113	13.4	49.3	10.8	0.24	9.2	1.5	9.2	1.9	6.1	0.93	6.2	0.98	6	55.6	12.6
PR5	Dolomit	Predazz	46°18'	11°36'	Biotite g	72.16	0.10	13.77	1.78	0.04	0.15	0.98	3.47	5.07	0.02	1.12	98.66	0.16	375	80	61	6.8	2	6	50	45	184	27	6	3.1	69.1	138	15	52.1	9.6	0.46	7.4	1.2	7.2	1.5	4.6	0.7	4.7	0.77	27	44.4	11

			.80"N	.60"E	anite																																																
PA13	Dolomites	Predazzo	46°18'29.85"N	11°36'17.06"E	Biotite granite	69.05	0.27	15.46	2.69	0.06	0.28	1.30	3.38	6.07	0.04	1.09	99.70		0.19		351	155	89	8	5	10	20	3		10	40	44	329	29	9	3	85	168	17.8	64	11.8	0.77	8.8	1.3	7.6	1.5	4.5	0.69	4.8	0.74	26	46.3	8.8
PA17	Dolomites	Predazzo	46°19'33.2	11°35'54.1	Albitized gran	72.48	0.08	13.36	1.12	0.02	0.06	1.01	3.04	6.07		1.30	98.53		0.11		418	21	34	6.5			20	9		120	50	55	177	26	6.4	3.5	62.9	138	15.4	55.3	12.3	0.27	10.7	1.8	10.6	1.9	5.7	0.92	6.4	0.96	11	64.9	14.1

			1"N	3"E	ite																																														
PA15	Dolomites	Monzoni	46°23'25.14"N	11°45'4.00"E	Gabbro	44.51	1.32	12.22	15.62	0.24	9.81	11.91	1.79	1.30	0.11	0.84	99.68	0.59	38	620	239	2.8	47	483	150	60	70	40	110	15	82	5	2.4	0.4	13.2	28.9	3.77	17.2	4.4	1.28	4.5	0.7	3.6	0.7	1.9	0.27	1.7	0.25	12	2.5	0.6
PA16	Dolomites	Monzoni	46°23'20.53"	11°44'57.47"	Gabbro (cumula	40.94	1.23	18.19	14.42	0.14	5.63	15.91	0.95	0.60	0.06	1.35	99.42	0.47	26	1008	85	2.9	40	527	30	49	60	630	80	9	44	2	1.7	0.2	8.2	19	2.57	12.6	3.1	0.99	3	0.4	2.4	0.5	1.2	0.17	1	0.17	11	1.7	0.5

			N	E	te)																																														
PA18	Dolomites	Monzoni	46°23'41.81"N	11°44'39.81"E	Olivinegabbros	48.85	1.26	17.40	10.83	0.17	5.32	8.55	3.72	1.50	0.39	2.14	100.10	0.52	39	1108	463	2.6	24	283	70	30	30	40	100	17	96	7	2.3	0.5	23.7	49.5	5.99	25.8	5.8	1.91	5	0.7	3.8	0.7	1.9	0.27	1.8	0.27	18	3	0.7
PA20	Dolomites	Monzoni	46°23'30.21"	11°44'30.07"	Olivinegabbros	48.21	1.37	16.85	12.52	0.20	6.30	11.03	2.69	1.22	0.34	0.10	100.80	0.53	25	891	343	0.9	35	277	80	41	40	20	110	18	64	6	2	0.5	21.7	45.6	5.9	25.7	5.7	1.83	5.3	0.7	4	0.7	2.1	0.3	1.8	0.26	6	1.3	0.3

			N	E																																															
PA21	Dolomites	Monzoni	46°23'34.71"N	11°44'10.35"E	Monzogabbros	46.43	1.60	16.85	13.94	0.21	5.89	10.46	2.64	1.62	0.69	0.33	100.70	0.49	38	1079	425	1.5	26	367	90	42	40	70	120	19	93	8	2.6	0.5	26.3	55.9	6.93	29.6	6.4	1.95	5.3	0.8	4.3	0.8	2.1	0.31	1.8	0.28	8	3.3	0.8
PA22A	Dolomites	Monzoni	46°23'32.43"N	11°43'34.29"E	Monzonites	55.51	0.90	17.19	9.06	0.19	2.89	6.56	3.47	3.12	0.36	1.05	100.30	0.42	127	819	557	3.4	15	159	20	22		50	100	27	167	12	3.9	1.1	36.7	77	9.14	37.6	7.4	1.79	6.6	1	5.5	1	3	0.44	2.8	0.46	12	9.6	2.6
P	D	M			M	5	0	1	8	0	2	5	3	3	0	1	9	0	1	8	5	5	1	1	2	1		5	9	2	1	1	4	1	3	7	8	3	6	1	6	0	5	1	2	0	2	0	1	9	2

A o o 4 1 o 6 . 7 . . . . 9 . 3 1 7 . 4 4 0 8 0 0 6 8 2 . 5 3 . 4 . . . . 7 . .
2 l n 6 1 n . 8 . 2 1 6 6 6 4 3 2 . 4 8 0 8 7 6 8 8 7 . 7 8 2 9 1 7 3 5 4 1 6
3 o z ° ° z 3 7 3 4 5 1 4 0 3 3 8 8 2 3 6 9 3
m o 2 4 o 9 4 8
i n 3 3 n
t i ' ' it
e 3 8 e
s 0 . s
. 4
0 0
4 "
" E
N

4
6 1
° 1
2 °
D 3 4 M
o ' 3 o
l M 3 ' n
o o 1 3 z 1
P m n . . o 5 1 0
A i z 4 4 n 6 0 7 8 0 2 5 3 4 0 1 0 0 3 7 8 1 0 0
2 t o 8 8 it . . . . 1 8 5 6 1 1 4 6 4 . 7 . 6 5 2 . 2 . 8 1
4 e n " " e 0 8 4 5 1 7 2 4 0 3 6 6 4 8 2 8 . 1 5 2 1 6 6 2 9 1 . . . 8 3 . 6 . . . 4 . 4 1 . .
s i N E s 8 6 3 1 6 0 5 7 9 7 5 0 2 0 1 2 3 3 7 0 9 0 0 6 0 3 7 1 2 7 9 6 1 5 2 1 4 1 8 1 7 3 2 6 9
H V V A 5 0 1 7 0 2 5 2 2 0 4 1 0 4 5 4 1 1 4 1 3 8 3 6 1 6 0 5 1 3 0 3 0 1 2
A i a 4 1 n 8 . 6 . . . . 0 . 8 0 4 . 1 6 2 1 1 9 2 8 1 . . 8 7 . 2 . . . . 1 1 .
c l 5 1 d . 9 . 2 1 4 4 3 6 2 1 0 4 1 9 1 9 9 5 0 4 0 0 9 0 2 6 2 . 6 4 . 9 7 3 9 6 1 2 4 1 4 9 . 8

7	entinian Alps	di Leder, Posina	°48'4.00"N	°14'58.00"E	esite	93	5	13	6	4	4	7	5	3	2	3	.70	3																	9		9	1		2						9		4		6	
HA1	Vicentinian Alps	Collegio, Laghi	45°49'46.12"N	11°16'43.40"E	Andesite	58.07	0.99	16.34	6.64	0.09	3.66	6.03	2.24	3.59	0.30	2.77	100.70	0.55	117	471	635	2.8	19	161	120	18	20	20	90	31	211	16	4.2	1.3	45.6	91.6	10.3	39.7	8	1.85	6.2	1	6	1.1	3.2	0.45	3	0.49	20	12.2	3.3

HA19	Vicentinian Alps	Trail to Busi, Schio	45°45'9.52"N	11°21'50.43"E	Latite	58.04	0.83	15.87	6.78	0.10	3.63	3.41	3.17	4.13	0.22	3.26	99.45	0.55	153	283	636	3.1	19	163	60	16	40	80	35	198	14	5.1	1.2	47.5	83.3	10.1	40.3	8.3	2.04	7.9	1.1	5.9	1.2	3.2	0.44	2.8	0.42	15	13.2	3.2
HA17	Vicentinian A	Contrà Lovati	45°45'29.57"	11°22'6.45"E	Dacite	63.81	0.55	15.66	4.95	0.09	1.24	4.27	2.23	3.93	0.21	3.15	100.10	0.36	159	402	825	5.7	12	70		8		80	32	200	13	5	1.4	50.8	98.2	10.6	38.9	7.9	1.76	6.9	1	5.9	1.1	3.5	0.51	3.4	0.5	25	14.9	3.6

HA9	Vicentinia	ord the South, Posina Bragioli, Po	45°48'23.	11°16'19.	Rhyolite	68.07	0.36	15.87	2.72	0.02	0.41	0.89	0.81	7.11	0.09	4.19	100.50	0.25	209	65	603	6.5	9	56	20	4	30	63	175	8	4.6	1.1	60.5	77.4	13.3	51.3	10.2	1.98	10.8	1.5	8.3	1.7	4.8	0.65	3.9	0.59	21	16.1	2.8

n	s	0	8
	i	9	8
A	n	"	"
l	a	N	E
p			
s			

Table 1. Major and trace-element contents of the studied samples from Dolomites and Vicentinian Alps.

	Rock Type	Measured data (with errors)										Age-corrected (230 Ma) values				
		87Sr/86Sr	±	143Nd/144Nd	±	206Pb/204Pb	±	207Pb/204Pb	±	208Pb/204Pb	±	87Sr/86Sr	143Nd/144Nd	206Pb/204Pb	207Pb/204Pb	208Pb/204Pb
GAR3	Subalkali Basalt	0.705364	0.000013	0.512490	0.000009	18.5295	0.0024	15.6618	0.0021	38.7766	0.0051	0.70508	0.51229	18.263	15.648	38.406
BUF2	Subalkali Basalt	0.705321	0.000009	0.512505	0.000008	18.5866	0.0012	15.6534	0.0010	38.7468	0.0024	0.70492	0.51230	18.296	15.639	38.356
LAT2	K-Alkali Basalt	0.706344	0.000007	0.512533	0.000009	19.4956	0.0137	15.6810	0.0107	39.0526	0.0263	0.70577	0.51234	18.353	15.674	38.894
BUF4	Potassic Trachybasalt	0.704583	0.000010	0.512561	0.000008	18.5329	0.0012	15.6522	0.0009	38.6292	0.0023	0.70432	0.51237	18.393	15.645	38.450
MAR1	Potassic Trachybasalt	0.704839	0.000009	0.512558	0.000010	18.5013	0.0039	15.6414	0.0035	38.7043	0.0084	0.70451	0.51236	18.337	15.633	38.483
DUR4	Shoshonite	0.705548	0.000008	0.512535	0.000006	18.4937	0.0012	15.6440	0.0009	38.5627	0.0024	0.70480	0.51234	18.406	15.640	38.455
PR3	Latite	0.706458	0.000007	0.512449	0.000009	18.4923	0.0005	15.6210	0.0004	38.5526	0.0011	0.70491	0.51227	18.398	15.616	38.434

Table 2. Sr-Nd-Pb radiogenic isotope values of representative samples

Highlights

The first complete review of the Middle Triassic magmatism of Southern Alps is presented

The composition of the igneous rocks indicates subduction-modified mantle sources

The geochemical message is at odds with the geological evidences of continental rifting stages.

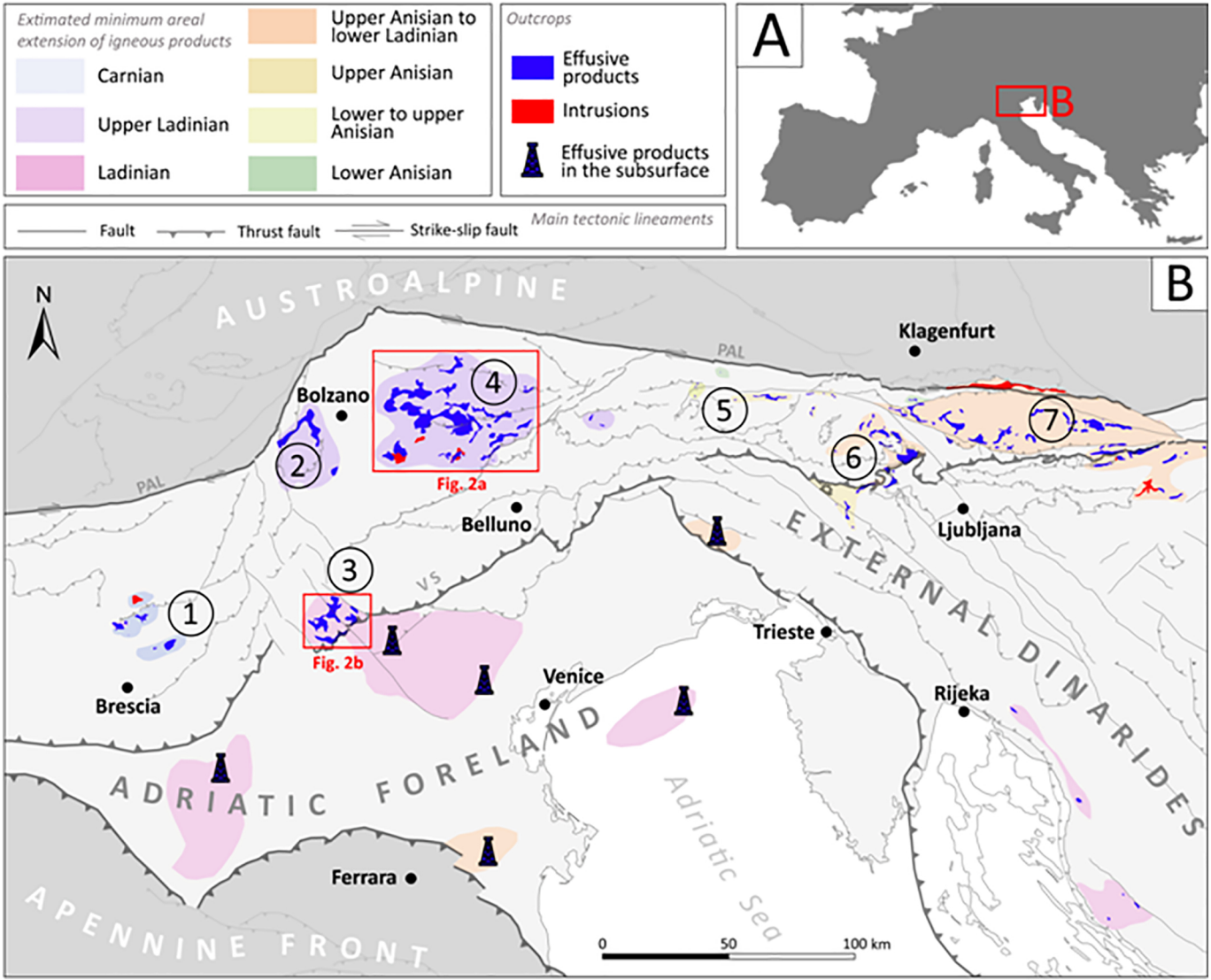
Extimated minimum areal extension of igneous products
Carnian
Upper Ladinian
Ladinian
Upper Anisian to lower Ladinian
Upper Anisian
Lower to upper Anisian
Lower Anisian
Outcrops
Effusive products
Intrusions
Effusive products in the subsurface
Fault
Thrust fault
Strike-slip fault
Main tectonic lineaments
A
B
N
AUSTROALPINE
PAL
Klagenfurt
Bolzano
Belluno
Ljubljana
Trieste
Rijeka
Venice
Brescia
Ferrara
Fig. 2a
Fig. 2b
VS
EXTERNAL DINARIDES
ADRIATIC FORELAND
APENNINE FRONT
Adriatic Sea
0
50
100 km
1
2
3
4
5
6
7

Figure 1

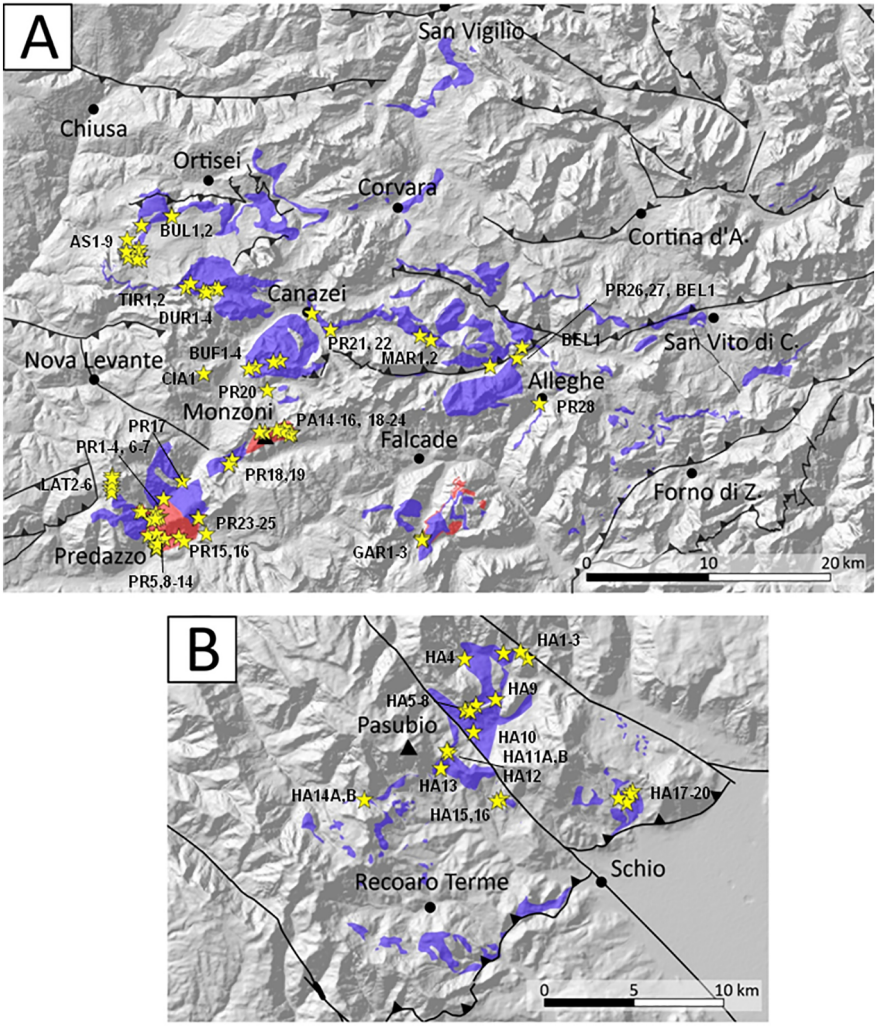
A
San Vigilio
Chiusa
Ortisei
Corvara
Cortina d'A.
AS1-9
BUL1,2
TIR1,2
DUR1-4
Canazei
PR26,27, BEL1
BEL1
San Vito di C.
PR21, 22
MAR1,2
BUF1-4
CIA1
Nova Levante
PR20
Alleghe
PR28
Monzoni
PA14-16, 18-24
Falcade
PR17
PR1-4, 6-7
PR18,19
LAT2-6
Forno di Z.
PR23-25
Predazzo
PR15,16
GAR1-3
PR5,8-14
0
10
20 km
B
HA1-3
HA4
HA9
HA5-8
Pasubio
HA10
HA11A,B
HA12
HA13
HA14A,B
HA15,16
HA17-20
Schio
Recoaro Terme
0
5
10 km

Figure 2

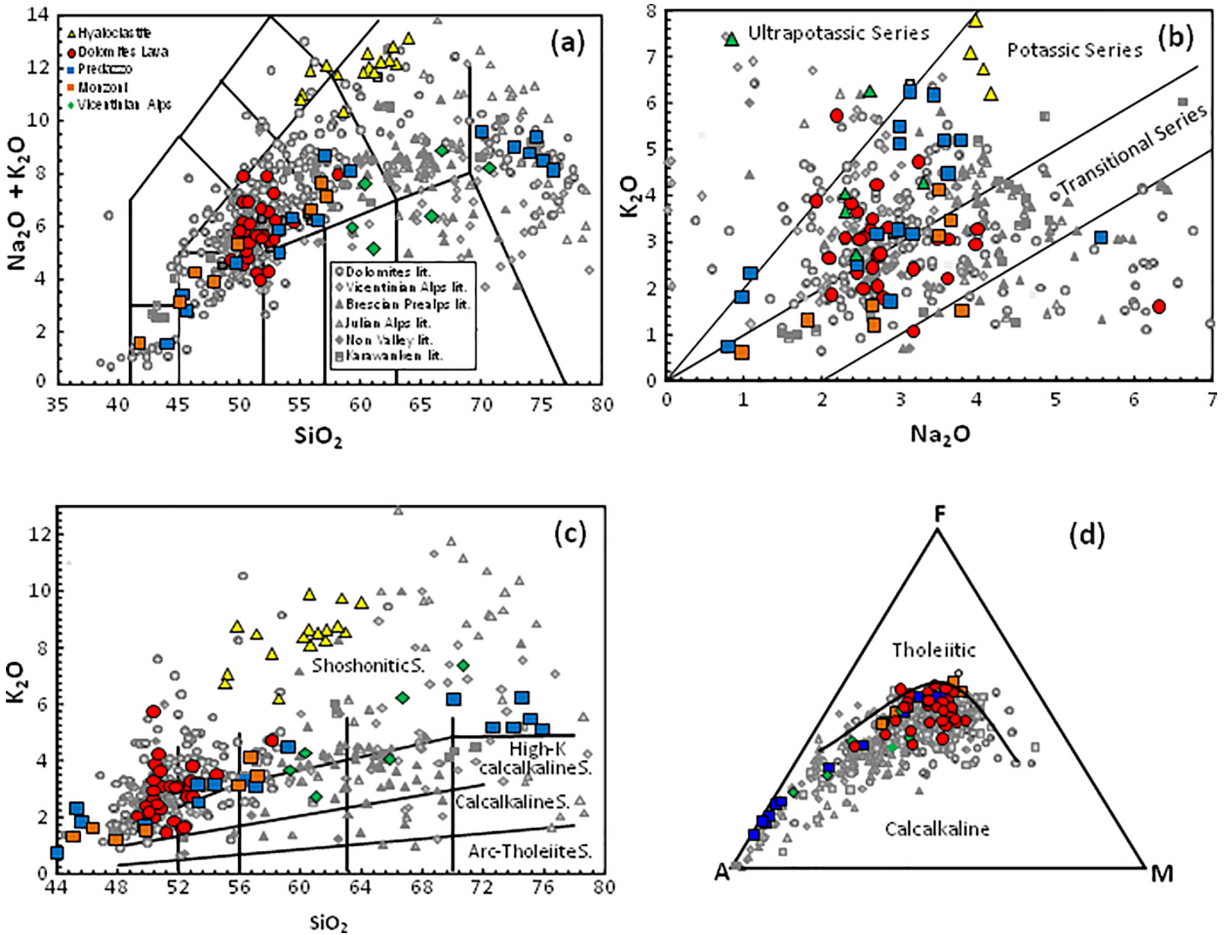
(a)
Hyaloclastite
Dolomites Lava
Predazzo
Monzoni
Vicentinian Alps
Dolomites lit.
Vicentinian Alps lit.
Brescian Prealps lit.
Julian Alps lit.
Non Valley lit.
Karawanken lit.
Na2O + K2O
SiO2
(b)
Ultrapotassic Series
Potassic Series
Transitional Series
K2O
Na2O
(c)
ShoshoniticS.
High-K calcalkalineS.
CalcalkalineS.
Arc-TholeiiteS.
K2O
SiO2
(d)
F
Tholeiitic
Calcalkaline
A
M

Figure 3

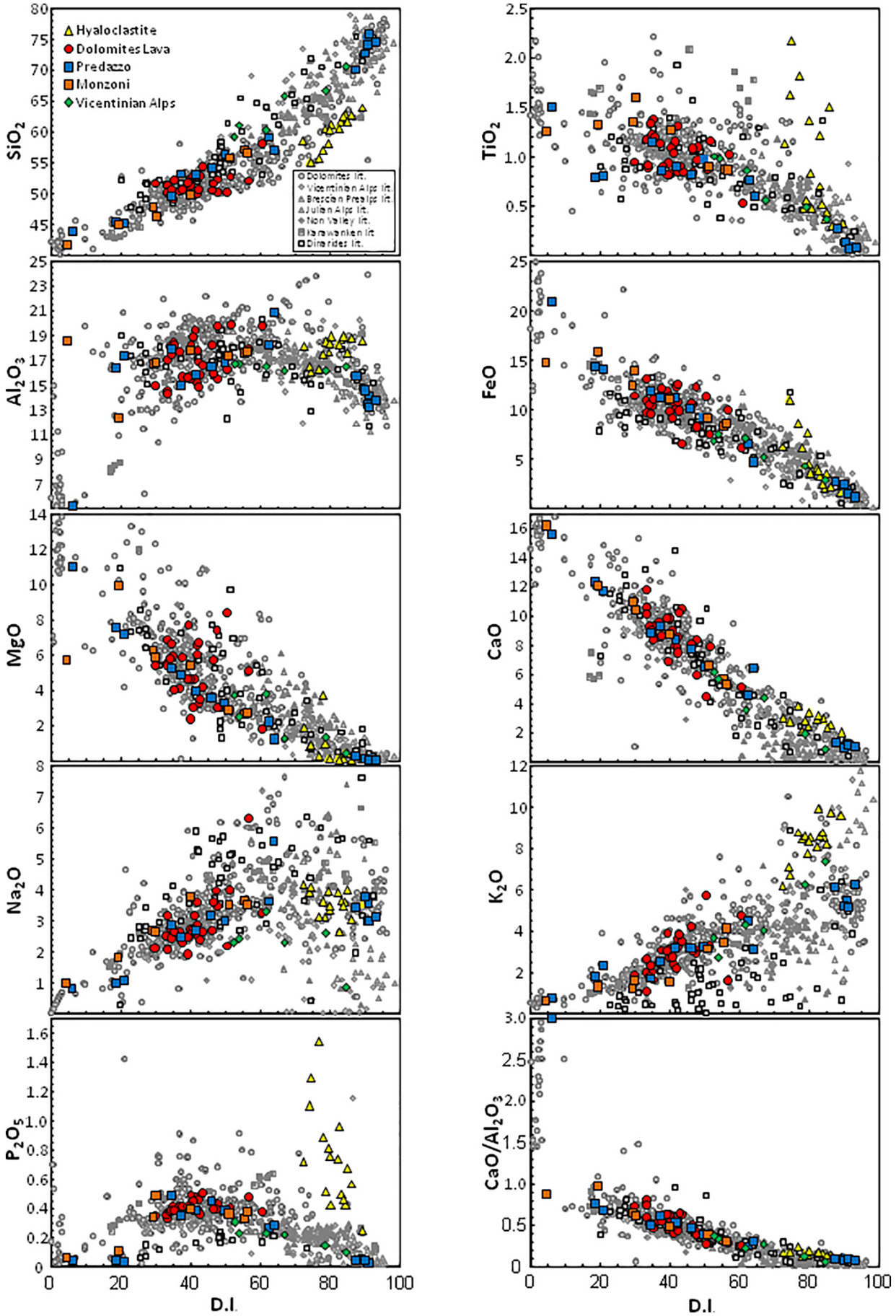
Hyaloclastite
Dolomites Lava
Predazzo
Monzoni
Vicentinian Alps
Dolomites lit.
Vicentinian Alps lit.
Brescian Prealps lit.
Julian Alps lit.
Non Valley lit.
Karawanken lit.
Dinarides lit.
SiO2
TiO2
Al2O3
FeO
MgO
CaO
Na2O
K2O
P2O5
CaO/Al2O3
D.I.
D.I.

Figure 4

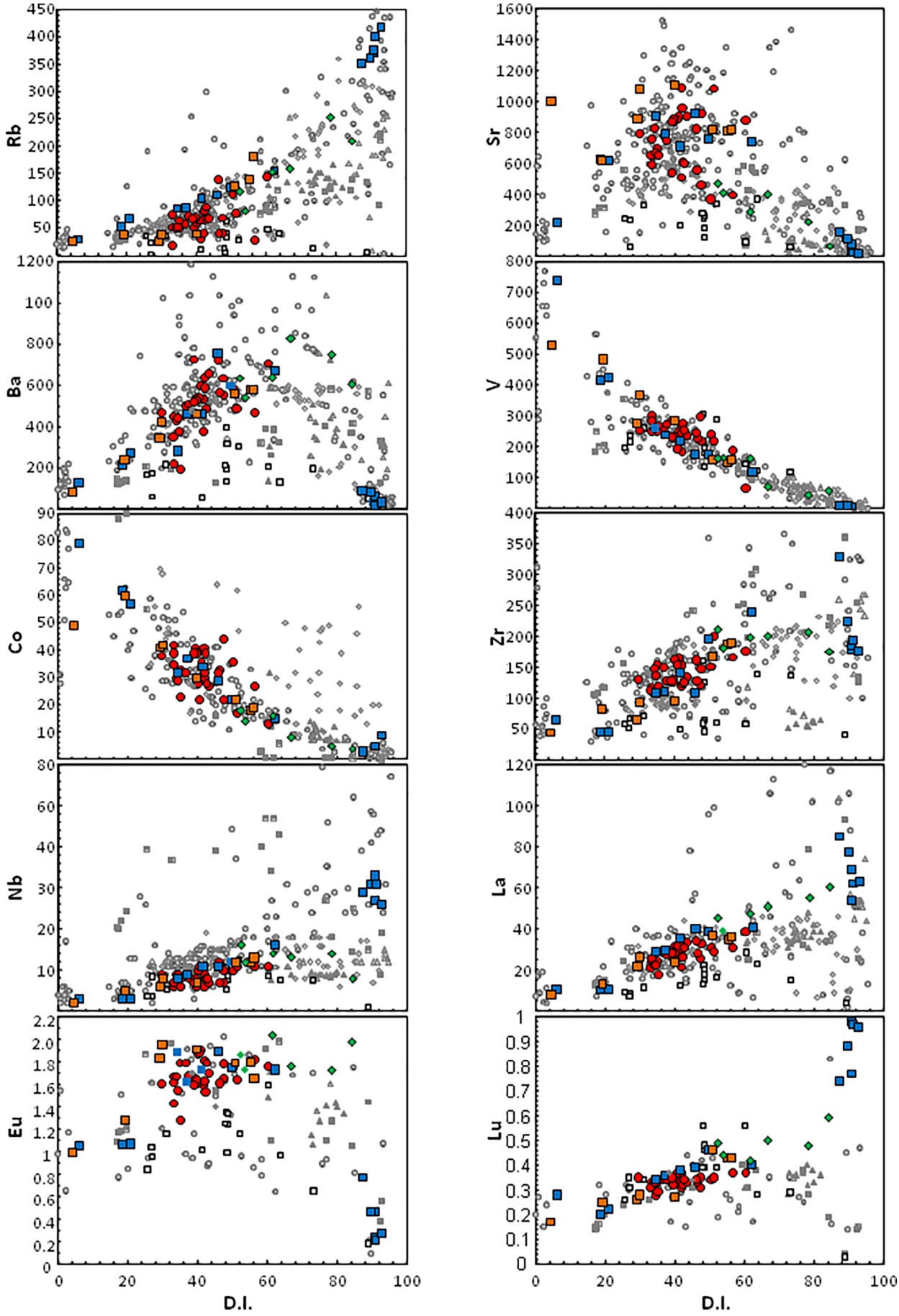

Figure 5

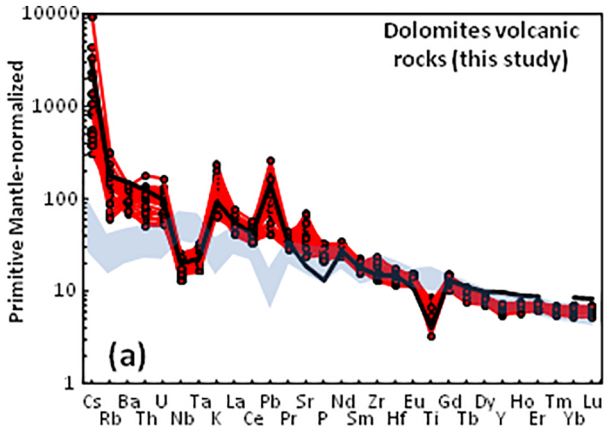
Dolomites volcanic rocks (this study)
Primitive Mantle-normalized
10000
1000
100
10
1
(a)
Cs Rb Ba Th U Nb Ta K La Ce Pb Pr Sr P Nd Sm Zr Hf Eu Ti Gd Tb Dy Y Ho Er Tm Yb Lu

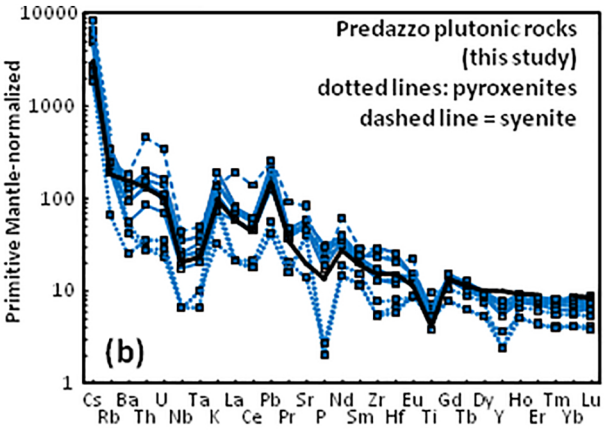
Predazzo plutonic rocks (this study)
dotted lines: pyroxenites
dashed line = syenite
Primitive Mantle-normalized
10000
1000
100
10
1
(b)
Cs Rb Ba Th U Nb Ta K La Ce Pb Pr Sr P Nd Sm Zr Hf Eu Ti Gd Tb Dy Y Ho Er Tm Yb Lu

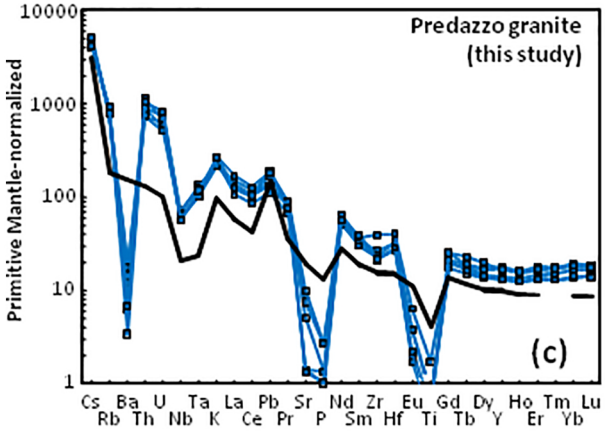
Predazzo granite (this study)
Primitive Mantle-normalized
10000
1000
100
10
1
(c)
Cs Rb Ba Th U Nb Ta K La Ce Pb Pr Sr P Nd Sm Zr Hf Eu Ti Gd Tb Dy Y Ho Er Tm Yb Lu

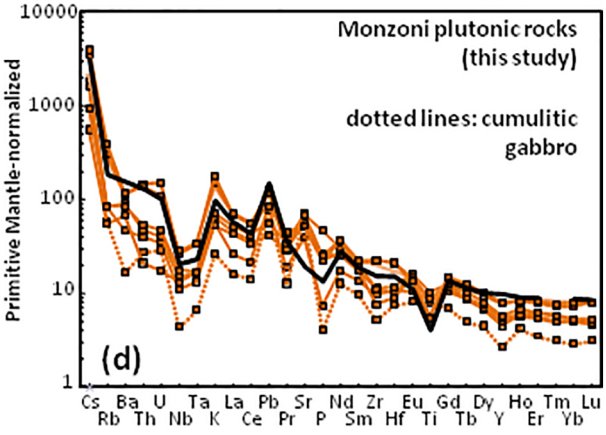
Monzoni plutonic rocks (this study)
dotted lines: cumulitic gabbro
Primitive Mantle-normalized
10000
1000
100
10
1
(d)
Cs Rb Ba Th U Nb Ta K La Ce Pb Pr Sr P Nd Sm Zr Hf Eu Ti Gd Tb Dy Y Ho Er Tm Yb Lu

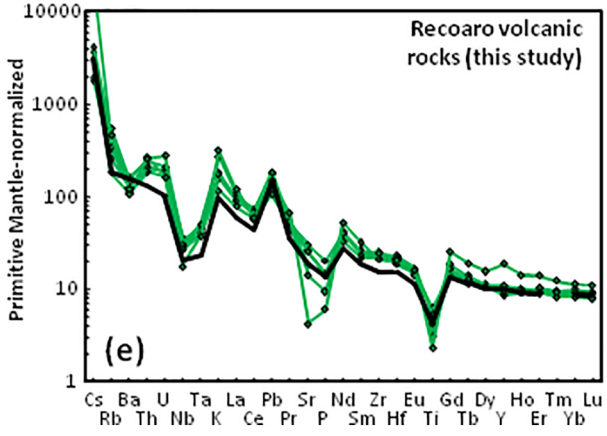
Recoaro volcanic rocks (this study)
Primitive Mantle-normalized
10000
1000
100
10
1
(e)
Cs Rb Ba Th U Nb Ta K La Ce Pb Pr Sr P Nd Sm Zr Hf Eu Ti Gd Tb Dy Y Ho Er Tm Yb Lu

Figure 6

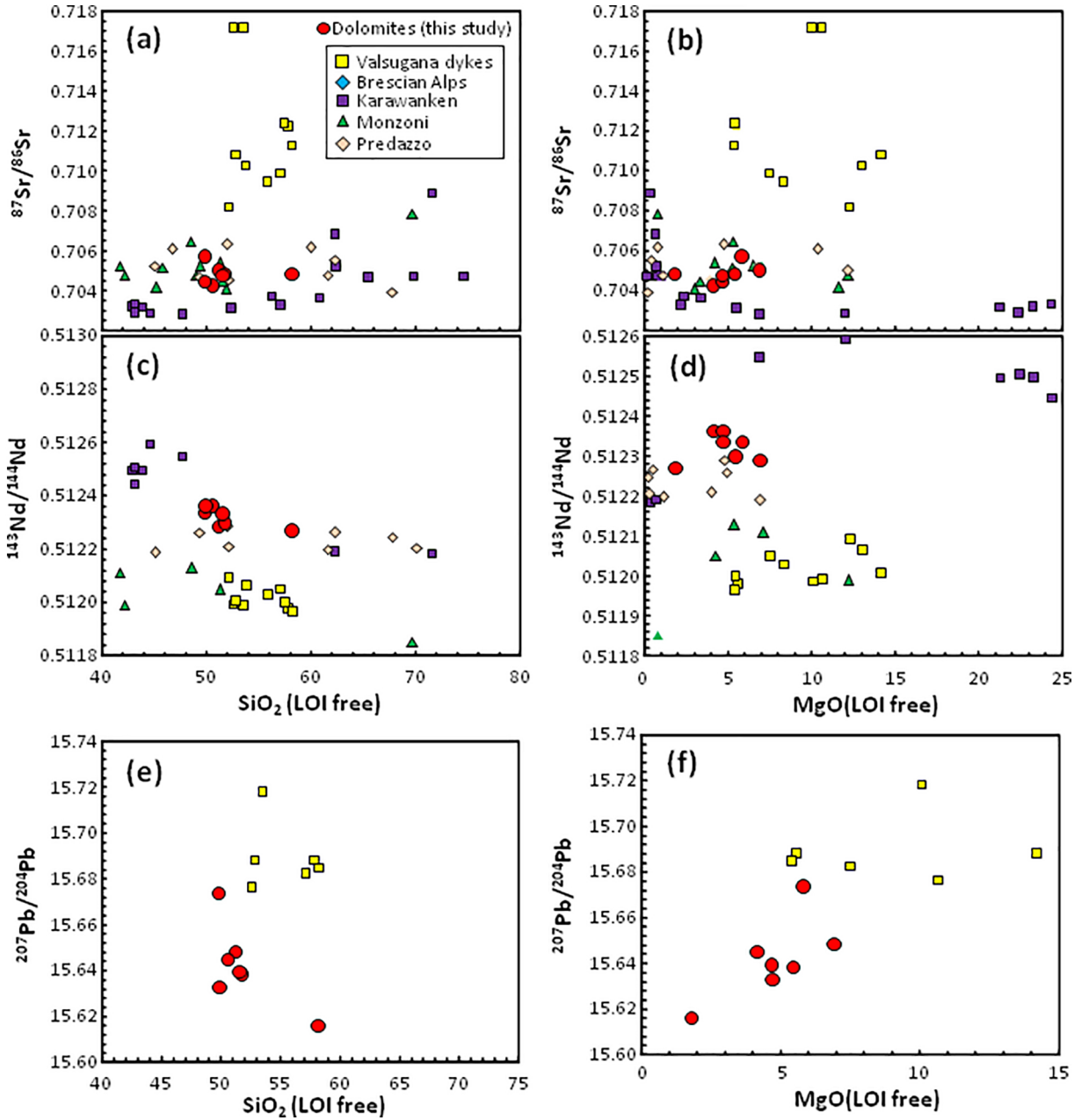
(a)
Dolomites (this study)
Valsugana dykes
Brescian Alps
Karawanken
Monzoni
Predazzo
$^{87}Sr/^{86}Sr$
(b)
$^{87}Sr/^{86}Sr$
(c)
$^{143}Nd/^{144}Nd$
SiO_2 (LOI free)
(d)
$^{143}Nd/^{144}Nd$
MgO(LOI free)
(e)
$^{207}Pb/^{204}Pb$
SiO_2 (LOI free)
(f)
$^{207}Pb/^{204}Pb$
MgO(LOI free)

Figure 7

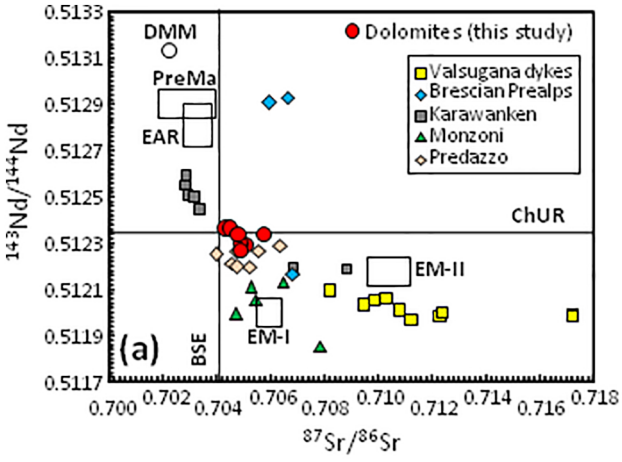
Dolomites (this study)
Valsugana dykes
Brescian Prealps
Karawanken
Monzoni
Predazzo
DMM
PreMa
EAR
ChUR
EM-II
EM-I
BSE
(a)
$^{143}Nd/^{144}Nd$
$^{87}Sr/^{86}Sr$

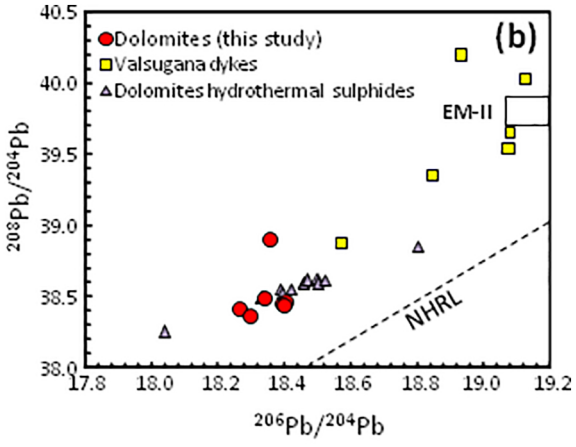
Dolomites (this study)
Valsugana dykes
Dolomites hydrothermal sulphides
(b)
EM-II
NHRL
$^{208}Pb/^{204}Pb$
$^{206}Pb/^{204}Pb$

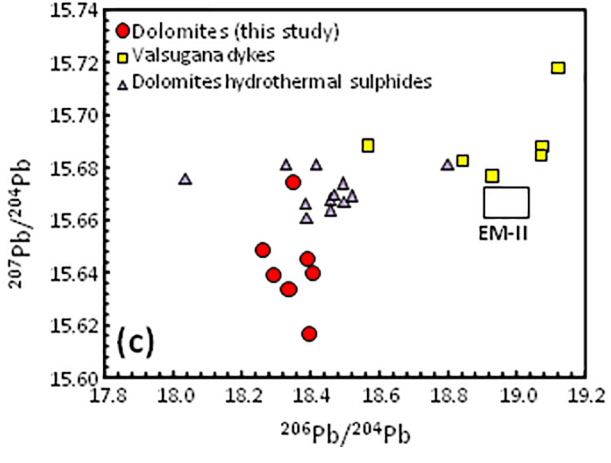
Dolomites (this study)
Valsugana dykes
Dolomites hydrothermal sulphides
EM-II
(c)
$^{207}Pb/^{204}Pb$
$^{206}Pb/^{204}Pb$

Figure 8

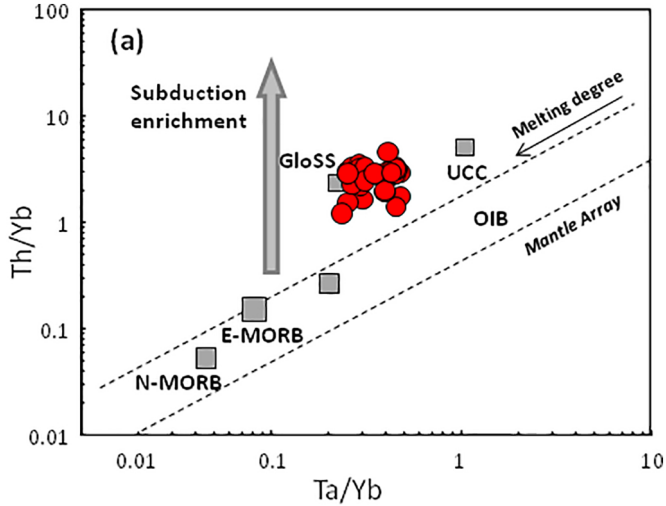
(a)
Subduction enrichment
GloSS
UCC
Melting degree
OIB
Mantle Array
E-MORB
N-MORB
Th/Yb
Ta/Yb
100
10
1
0.1
0.01
0.01
0.1
1
10

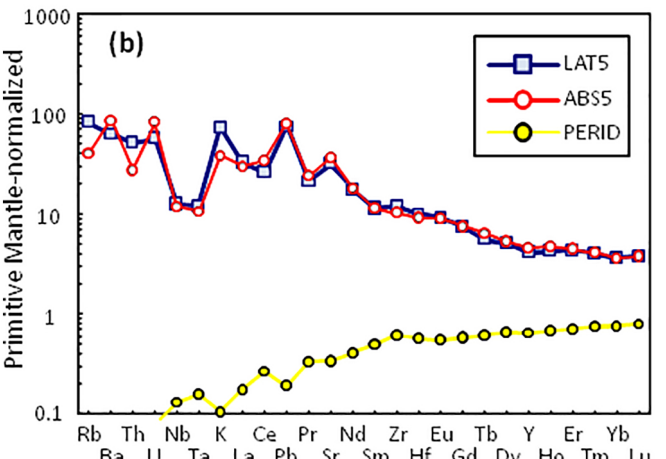
(b)
LAT5
ABS5
PERID
Primitive Mantle-normalized
1000
100
10
1
0.1
Rb Th Nb K Ce Pr Nd Zr Eu Tb Y Er Yb
Ba U Ta La Pb Sr Sm Hf Gd Dy Ho Tm Lu

Figure 9